

*Gradu Amaierako Lana/Trabajo Fin de Grado*

**Fisikako Gradua/Grado en Física**

---

# Quantum Illumination Protocols

---

**Borja Ramón Gómez**

*Director:*

**Prof. Enrique Solano**

*Codirector:*

**Dr. Mikel Sanz**



Department of Physical Chemistry  
Faculty of Science and Technology  
University of the Basque Country UPV/EHU

Leioa, June 2019



# Contents

<b>Contents</b>	<b>3</b>
<b>1 Fundamentals of Gaussian Quantum Illumination</b>	<b>7</b>
1.1 Gaussian Quantum States . . . . .	7
1.1.1 Wigner-Weyl Transform . . . . .	8
1.1.2 Gaussian State Description . . . . .	9
1.1.3 Graphic Representation of Gaussian States . . . . .	10
1.2 Beam Splitter . . . . .	11
<b>2 Quantum Illumination Protocol</b>	<b>15</b>
2.1 Classical Protocol . . . . .	16
2.2 Quantum Protocol . . . . .	18
2.3 Comparison . . . . .	21
2.4 Quantum Radar . . . . .	22
2.4.1 Optical vs Microwave Regime . . . . .	23
<b>3 Photon Subtraction</b>	<b>25</b>
3.1 PS on a Two-Mode Squeezed State . . . . .	26
3.2 PS on Single-Mode Gaussian States . . . . .	28
3.3 PS with Optimal Displacement and Squeezing . . . . .	33
<b>Bibliography</b>	<b>39</b>
<b>Appendices</b>	<b>41</b>
<b>A Intermediate Calculations</b>	<b>43</b>
A.1 Optimal Photon Reduction . . . . .	43
A.2 Optimal PS Protocol Expectation Values . . . . .	43
<b>B Mathematica Programs</b>	<b>47</b>
B.1 Representation in Phase Space of different Wigner Functions	47
B.2 Representation of SNR Comparisons . . . . .	49
B.3 Optimal Displacement and Squeezing Calculation and Graphic Representation . . . . .	52

B.4 Gaussian VS Optimal PS Comparison . . . . . 57

# Introduction and Objectives

In the early 20th century, quantum mechanics arose aiming at explaining some phenomena in disagreement with the predictions given by the classical theories. This led to the so-called first quantum revolution, where several technologies, for which the quantum theory is essential, such as lasers, semiconductor-based transistors, superconducting magnets, etc. were developed. These devices, which have certainly revolutionized the world, require quantum physics to explain how they work, but the codified information is classical.

The emergence and rapid development of quantum technologies due to the increasing interest leads us towards the second quantum revolution. A much more precise control of the technology allows us to manipulate quantum states of matter and employ quantum effects such as superposition and entanglement to develop practical applications. We can roughly divide these technologies into three main pillars: computation, communication and sensing. This work will mainly focus on the last one, namely, quantum sensing.

In quantum sensing, we take advantage of the peculiar properties of quantum mechanics to develop more precise measurement devices. Paradigmatic examples are atomic clocks or atom interferometers, which do not make use of entanglement and are already commercial devices. There are also entanglement-based metrology devices, which promise much higher precision than the limit classically obtainable. The quantum radar is a remarkable example of a technology which could improve the detection of the presence of an object in space making use of quantum entanglement as a resource, and it is based on quantum illumination [1]. The objective of this work is to explain the concept of quantum illumination, showing its fundamental elements and the advantage over classical protocols for different quantum states, both with Gaussian and non-Gaussian ones. In Chapter 1, we introduce the fundamentals of quantum illumination. After explaining the phase-space formulation of quantum optics, we introduce Gaussian states, fundamental in these protocols.

In Chapter 2, the optimal protocols in classical and quantum illumination are explained and compared by making use of a figure of merit called signal-to-noise ratio (SNR). In this Chapter, the quantum protocol is realized with a particularly relevant Gaussian state called two-mode squeezed state. We

also present the concept of quantum radar and its relation with quantum illumination.

Finally, after showing the advantage of the quantum Gaussian protocol, we introduce in Chapter 3 a new tool called photon subtraction, an operation that takes the Gaussian state out of this set of quantum states, which is supposed to improve the quantum protocol's performance [2]. Gaussian and non-Gaussian protocols are carefully compared in order to check whether the photon subtraction technique provides a real benefit or not.

To sum up, in this work I have understood what Gaussian states are and the fundamentals of quantum illumination with them as the resource, as well as to compute the performance of different protocols and to compare them. In this process, I have deepened in the use of Mathematica, with which I have computed the SNR of the protocols and depicted all the graphics in this work. All the written Mathematica programs are exposed in the Appendix.

# Chapter 1

## Fundamentals of Gaussian Quantum Illumination

Quantum illumination is a detection scheme which takes advantage of quantum entanglement to achieve enhancement, either in the error probability or in the resources employed, over the classical protocol [3]. A remarkable feature shown by this paradigm when compared against other quantum information applications, such as superdense coding or quantum teleportation, is that the quantum advantage survives even in highly noisy environments, in which quantum entanglement is a fragile property [4].

In Section 1.1, we introduce Gaussian quantum states of the quantum harmonic oscillator, a family of quantum states commonly utilized in quantum information, and specially in quantum illumination [5]. Quantum states and observables are commonly presented as Hilbert space operators but, in order to properly define Gaussian quantum states, we will need an alternative description, called phase-space formulation.

Finally, in Section 1.2, we present the beam splitter, a key device in quantum optics for the generation of entanglement.

### 1.1 Gaussian Quantum States

Gaussian quantum states are a family of states of the quantum harmonic oscillator, and an essential class of quantum states in quantum information with continuous variables, i.e. with systems with continuous physical observables. Their relevance in quantum information is due to the fact that they are easy to experimentally prepare and manipulate. Furthermore, their mathematical definition only depends on its first and second canonical moments, as we will see later in its definition.

In order to properly define Gaussian states, an understanding of their phase-space formulation is needed. This representation of states is achieved through the Wigner-Weyl transform.

### 1.1.1 Wigner-Weyl Transform

The Wigner-Weyl transform (after Eugene Wigner and Hermann Weyl) is the relation required to depict quantum states and operators in phase-space [6]. Characterizing operators and states in phase space implies the conversion of an operator to a function dependent on  $x$  and  $p$ , and this is performed through the Weyl transform.

The Weyl transform is the representation of an operator in phase-space, and, for the 1-dimensional case, it is defined as

$$\begin{aligned}\tilde{A}(x, p) &= \int e^{-ipy/\hbar} \langle x + y/2 | \hat{A} | x - y/2 \rangle dy \\ &= \int e^{-ixq/\hbar} \langle p + q/2 | \hat{A} | p - q/2 \rangle dq.\end{aligned}\quad (1.1)$$

Quantum states are represented in the same manner as operators, but replacing the operator  $\hat{A}$  by the density operator  $\hat{\rho}$  divided by the Planck constant. For a pure state  $\hat{\rho} = |\Phi\rangle\langle\Phi|$ , the Wigner function is defined by

$$\begin{aligned}W(x, p) &= \int e^{-ipy/\hbar} \langle x + y/2 | (\hat{\rho}/\hbar) | x - y/2 \rangle dy \\ &= \frac{1}{\hbar} \int e^{-ipy/\hbar} \langle x + y/2 | \Phi \rangle \langle \Phi | x - y/2 \rangle dy \\ &= \frac{1}{\hbar} \int e^{-ipy/\hbar} \Phi(x + y/2) \Phi^*(x - y/2) dy.\end{aligned}\quad (1.2)$$

The definition of the Wigner function is easily generalized to mixed states. As  $\hat{\rho} = \sum_i P_i |\Phi_i\rangle\langle\Phi_i|$ ,

$$W(x, p) = \frac{1}{\hbar} \int e^{-ipy/\hbar} \sum_i P_i \Phi_i(x + y/2) \Phi_i^*(x - y/2) dy = \sum_i P_i W_i(x, p).\quad (1.3)$$

One of the most important properties of the Weyl transform is that  $\text{Tr}[\hat{A}\hat{B}]$ , the trace of the product of two operators, is given by the expression

$$\text{Tr}[\hat{A}\hat{B}] = \frac{1}{\hbar} \iint \tilde{A}(x, p) \tilde{B}(x, p) dx dp.\quad (1.4)$$

From Eq. 1.4, obtaining the expectation value of an observable  $A$  is straightforward,

$$\langle A \rangle = \text{Tr}[\hat{A}\hat{\rho}] = \iint W(x, p) \tilde{A}(x, p) dx dp.\quad (1.5)$$



The Wigner function also provides a simple technique to obtain the probability distribution for the position as well as for the momentum. This is achieved by projecting  $W(x, p)$  on the  $p$ -axis and  $x$ -axis respectively:

$$|\phi(x)|^2 = \phi^*(x)\phi(x) = \int W(x, p)dp, \quad (1.6)$$

$$|\phi(p)|^2 = \phi^*(p)\phi(p) = \int W(x, p)dx. \quad (1.7)$$

### 1.1.2 Gaussian State Description

Let us now define Gaussian states using the recently learnt phase-space formulation. Given a quantum state  $\hat{\rho}$ , the vector of first moments  $\langle \mathbf{r} \rangle$  and the covariance matrix  $\sigma_{ij}$  are respectively defined as

$$\langle \mathbf{r} \rangle_{\rho} = Tr[\hat{\rho}\hat{\mathbf{r}}], \quad (1.8)$$

$$\sigma_{ij} = \langle \{r_i, r_j\} \rangle_{\rho} - 2 \langle r_i \rangle_{\rho} \langle r_j \rangle_{\rho}, \quad (1.9)$$

where  $\mathbf{r}$  is defined as the vector of quadratures. Its dimension is  $2n$ , with  $n$  the number of modes in our system, i.e. the number of harmonic oscillators involved and 2 for the quadratures  $x$  and  $p$  of each mode. In the case of a single-mode state,  $\hat{\mathbf{r}} = (\hat{x}, \hat{p})$ . Then,  $\langle \mathbf{r} \rangle$  represents a vector whose components are the expectation values of both quadratures,  $\langle \mathbf{r} \rangle = (\langle x \rangle, \langle p \rangle)$ . A quantum state of a harmonic oscillator whose Wigner function has the form

$$W_{\rho}(\mathbf{r}) = \frac{1}{\pi^2 \sqrt{\det[\sigma]}} e^{-(\mathbf{r} - \langle \mathbf{r} \rangle)^T \sigma^{-1} (\mathbf{r} - \langle \mathbf{r} \rangle)}. \quad (1.10)$$

is called Gaussian quantum state [7].

The evolution of a density operator under a given Hamiltonian  $H$  is given by the relation  $\hat{\rho}(t) = e^{-i\hat{H}t} \hat{\rho} e^{i\hat{H}t}$ . In particular, we are interested in characterizing the Hamiltonians which preserve the Gaussian structure, i.e. which evolve Gaussian states into Gaussian states. The most general form of a Hamiltonian which conserves the Gaussian form of the Wigner function, in other words, which is Gaussian-preserving, is [7]

$$\hat{H} = \sum_{k=1}^n g_k^{(1)} \hat{a}_k^{\dagger} + \sum_{k>l=1}^n g_{kl}^{(2)} \hat{a}_k^{\dagger} \hat{a}_l + \sum_{k,l=1}^n g_{kl}^{(3)} \hat{a}_k^{\dagger} \hat{a}_l^{\dagger} + H.c., \quad (1.11)$$

where  $H.c.$  means Hermitian conjugate and  $n$  is the number of modes of the system. Any Gaussian state can be obtained by evolving unitarily a thermal state through a Hamiltonian given in Eq. 1.11, as it is shown in Ref. [8]. For

single-mode Gaussian states, a thermal state, which is already Gaussian, is described with the density matrix

$$\rho_{\text{th}} = (1 - \lambda) \sum_{n=0}^{\infty} \lambda^n |n\rangle\langle n|, \quad (1.12)$$

where  $\lambda$  is a real positive parameter smaller than 1. This parameter is determined by the temperature of our system and the frequency of the photons. Thermal states are usually defined by the expected number of photons  $n_{\text{th}} = \langle N \rangle = \lambda/(1 - \lambda)$ . In the case of a single mode, Eq. 1.11 transforms into

$$\hat{H}_1 = g^{(1)}\hat{a}^\dagger + g^{(3)}\hat{a}^{\dagger 2} + H.c. \quad (1.13)$$

This means that, from a thermal state (Eq. 1.12), we can generate any single-mode Gaussian state by applying a unitary evolution given by Eq. 1.13. The term  $g^{(1)}\hat{a}^\dagger + H.c.$  corresponds to the evolution given by the so-called displacement operator

$$\hat{D}(\alpha) = \exp\left(\alpha\hat{a}^\dagger - \alpha^*\hat{a}\right), \quad (1.14)$$

while the term  $g^{(3)}\hat{a}^{\dagger 2} + H.c.$  corresponds to the evolution described by the squeezing operator

$$\hat{S}(\xi) = \exp\left(\frac{1}{2}(\xi^*\hat{a}^2 - \xi\hat{a}^{\dagger 2})\right), \quad (1.15)$$

with both  $\alpha$  and  $\xi$  complex parameters. Then, a general Gaussian state in the operator representation can be written as [8]

$$\hat{\rho}_{\text{Gaussian}} = \hat{D}(\alpha)\hat{S}(\xi)\hat{\rho}_{\text{th}}\hat{S}^\dagger(\xi)\hat{D}^\dagger(\alpha). \quad (1.16)$$

To sum up, any single-mode Gaussian state can be determined by two complex numbers,  $\alpha$  and  $\xi$ , corresponding to the displacement and the squeezing respectively, and the number of thermal photons,  $n_{\text{th}}$ .

### 1.1.3 Graphic Representation of Gaussian States

It is very interesting and clarifying to represent different Gaussian states in phase-space. This allows us to understand the effect of the unitary operations of displacement and squeezing when acting on any Gaussian state.

The Wigner function of the thermal state is obtained by substituting Eq. 1.12 in Eq. 1.3, which results in

$$W_\lambda(x, p) = \frac{(1 - \lambda)}{\pi(\lambda + 1)\hbar} e^{-\frac{(1-\lambda)(p^2+x^2)}{(\lambda+1)\hbar}}. \quad (1.17)$$

The thermal state is represented in Fig. 1.1a.

The width and height of the Gaussian distribution depends on the number of thermal photons, and it is centred in the origin. From now on, we will apply unitary operations on the vacuum state  $|0\rangle\langle 0|$ , which is a particular case of a thermal state with  $\lambda = 0$ . Its representation in phase-space is therefore the narrowest among thermal states.

Applying the displacement operator given in Eq. 1.14 to a thermal state results in a displacement of the Wigner function in phase-space in the direction given by  $\alpha$ . Starting from the vacuum state, we generate an state called coherent state, given by

$$W_\alpha(x, p) = \frac{1}{\pi\hbar} e^{-\frac{\left(p - \frac{\text{Im}(\alpha)}{\sqrt{2\hbar}}\right)^2 + \left(x - \frac{\text{Re}(\alpha)}{\sqrt{2\hbar}}\right)^2}{\hbar}}, \quad (1.18)$$

which is represented in phase-space in Fig. 1.1b.

Regarding the squeezing operator (Eq. 1.15), it expands the distribution in a certain direction and stretches it in the perpendicular one. The squeezing operator acting on a vacuum state generates a squeezed vacuum state, given by

$$W_\xi(x, p) = \frac{1}{\pi\hbar} e^{-\frac{|(ip+x)\cosh(r) + e^{2i\theta}(-ip+x)\sinh(r)|^2}{2\hbar}}, \quad (1.19)$$

where  $r$  and  $\phi$  are the modulus and phase of  $\xi$  respectively. It is represented in Fig. 1.1c.

## 1.2 Beam Splitter

Quantum entanglement is a resource to exploit for different purposes, in our case, for quantum illumination. Until now, we have focused on single-mode operations. Let us now discuss entangling operations in two-mode systems. There are available a wide variety of entanglement-generating devices, but the beam splitter is the most paradigmatic device in quantum optics. We will consider a lossless beam splitter, therefore characterized by a unitary evolution. The transformation generated by this device can be described in the Heisenberg picture by a linear transformation of the annihilation operators of the modes,

$$\begin{pmatrix} \hat{b}_1 \\ \hat{b}_2 \end{pmatrix} = \begin{pmatrix} t_1 & r_1 \\ r_2 & t_2 \end{pmatrix} \begin{pmatrix} \hat{a}_1 \\ \hat{a}_2 \end{pmatrix}, \quad (1.20)$$

where  $t$ ,  $t'$  and  $r$ ,  $r'$  are complex transmission and reflection amplitude coefficients. They obey the constrains  $|r_1|^2 + |t_1|^2 = 1$ ,  $|r_1| = |r_2|$ ,  $|t_1| = |t_2|$ .

The Gaussian-preserving Hamiltonian of Eq. 1.11 for our two-mode system contains two additional terms which were not present in the single-mode case. One of them is  $\propto \hat{a}^\dagger \hat{a}$ , which causes a phase shift. However, the

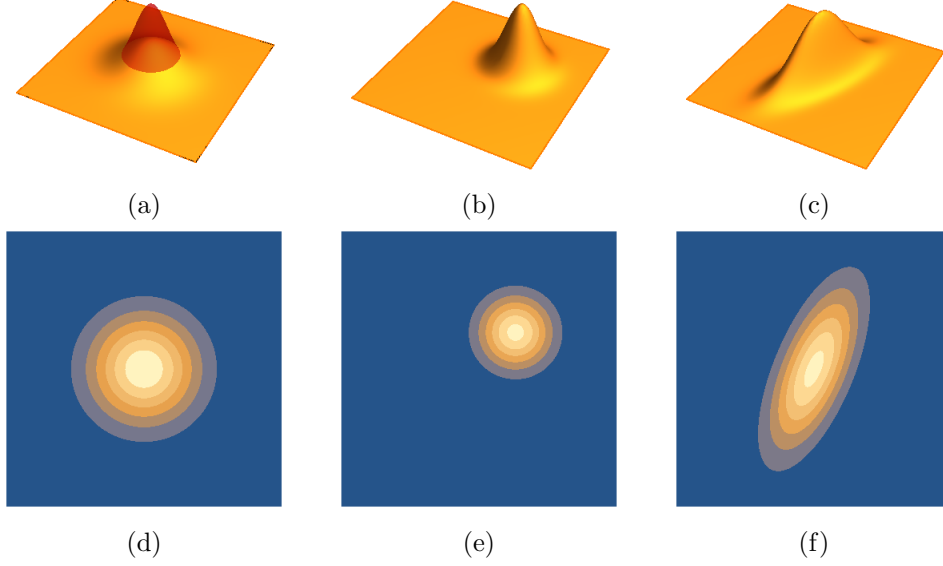


Figure 1.1: **Representation in phase space  $(x, p)$  of the Wigner function of different states.** The top graphics are 3-dimensional representations of different functions and the bottom ones are their respective contour plots. In (a), we have plotted the Wigner functions of a thermal state (Eq. 1.17) (orange) and a vacuum state (red), which is a thermal state with  $\lambda = 0$ . It can be seen that the distribution widens and the height decreases as  $\lambda$  increases. They are centred in the origin,  $(x, p) = (0, 0)$ . Figure (d) represents the contour plot of the Wigner function of a general thermal state. Figure (b) shows the Wigner function of a coherent state (Eq. 1.18). It is similar to the distribution for the vacuum state but its centre is displaced from the origin,  $(x, p) = (\text{Re}(\alpha), \text{Im}(\alpha))$ . The contour plot of the function is shown in (e). The last distribution, (c), corresponds to a squeezed vacuum state (Eq. 1.19). It is centred in the origin and its width is reduced in a direction and increased in the perpendicular one with respect to the vacuum state. Its contour plot is represented in Fig. (f).

interesting term is the mode mixing one,  $\propto \hat{a}_1^\dagger \hat{a}_2 + H.c.$ , which is precisely a beam splitter interaction, as we will see.

In Fig. 1.2, a schematic representation of a beam splitter is shown. The input fields are described by their respective annihilation operators  $\hat{a}_1$  and  $\hat{a}_2$ , and the output fields are described by  $\hat{b}_1$  and  $\hat{b}_2$ .

The transformation held by 1.20 can be also expressed as

$$\hat{b}_i = \hat{B} \hat{a}_i \hat{B}^\dagger, \quad i = 1, 2, \quad (1.21)$$

where the unitary beam splitter operator  $\hat{B}$  is

$$\hat{B} = \exp \left[ \frac{\theta}{2} (\hat{a}_1^\dagger \hat{a}_2 e^{i\phi} - \hat{a}_1 \hat{a}_2^\dagger e^{-i\phi}) \right]. \quad (1.22)$$

The beam splitter transformation is then described by 2 parameters.

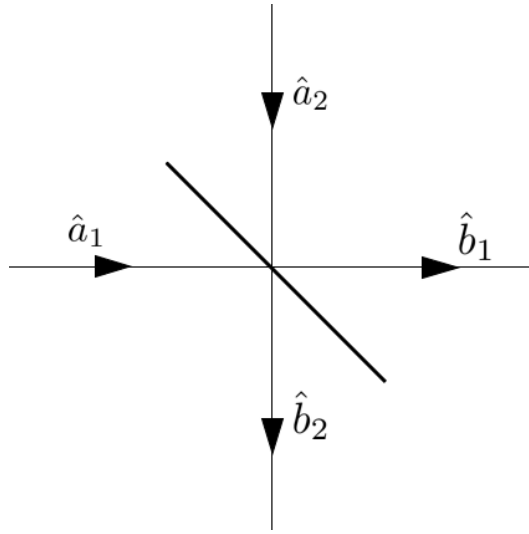


Figure 1.2: **Representation of the inputs ( $\hat{a}_1, \hat{a}_2$ ) and outputs ( $\hat{b}_1, \hat{b}_2$ ) of a beam splitter.** The unitary transformation generated by this device in the inputs is given by Eq. 1.22

$\theta \in [0, \pi/2]$  is related with the amplitude coefficients of reflection ( $r = \sin(\theta/2)$ ) and transmission ( $t = \cos(\theta/2)$ ) and  $\phi \in [0, \pi]$  gives the phase difference introduced by the beam splitter between the reflected fields and the transmitted ones.



## Chapter 2

# Quantum Illumination Protocol

In this Chapter, we explain the quantum entanglement-assisted protocol to detect the presence of an object. Indeed, we describe the quantum state preparation, the modelling of the interaction with the hypothetical object and the selection of an appropriated observable to be measured which provides an advantage with respect to the best classical protocol.

Additionally, we demonstrate the advantages of a quantum illumination protocol. For this aim, we firstly describe the classical protocol in Section 2.1 and the quantum one in Section 2.2. The states of quantum state preparation and measurement will be different in both protocols, since they are chosen in order to achieve the optimal classical and quantum protocols. Otherwise, the comparison would not be fair. A figure of merit, the signal-to-noise ratio (SNR), is calculated for both cases to have an idea of their efficiencies. Finally, both protocols are compared in Section 2.3 identifying the region of parameters in which the quantum protocol overcomes the classical one.

The SNR, is defined as the ratio of the power of the signal received and the power of the noise, so this gives us an idea of how much our signal stands out against the background. There is an alternative mathematical definition,

$$\text{SNR} = \frac{\mu^2}{\sigma^2} = \frac{\langle \hat{O} \rangle^2}{\langle \hat{O}^2 \rangle - \langle \hat{O} \rangle^2}, \quad (2.1)$$

which is the ratio of the mean or expected value squared,  $\mu^2$ , to the variance,  $\sigma^2$ . In the second equality, it is expressed with respect to a given observable  $\hat{O}$ .

Finally, in Section 2.4, we will briefly introduce the quantum radar technology, a generalization quantum illumination, and perform a qualitative comparison between the use of photons in the optical and microwave regimes.

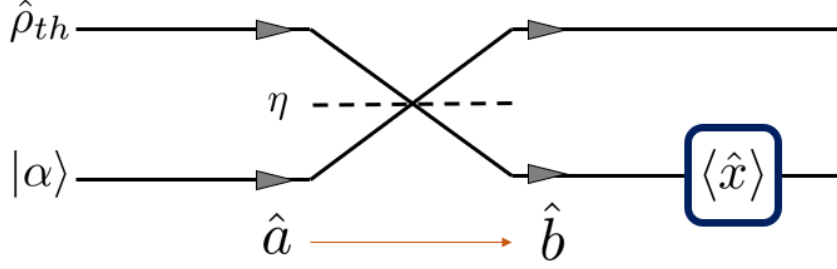


Figure 2.1: **Scheme of the classical protocol for target detection.** First, a coherent state is mixed with a thermal state through a low reflectivity beam splitter. Then, the measurement of the quadrature  $\hat{x}$  (Eq. 2.4) is realized. The orange arrow represents the change produced by the beam splitter on the fields (Eq. 2.3), represented by their respective annihilation operators.

## 2.1 Classical Protocol

An illumination protocol consists of three clearly distinguishable stages: the preparation of the quantum states (resource), the interaction with the environment and the object, and the measurement. In this Section, we describe them in detail. For a global and schematic overview of the classical protocol, see Fig. 2.1.

For the classical protocol, our resource is a coherent state

$$|\alpha\rangle = e^{-\frac{|\alpha|^2}{2}} \sum_{n=0}^{\infty} \frac{\alpha^n}{\sqrt{n!}} |n\rangle, \quad (2.2)$$

which is the application of the displacement operator (Eq. 1.14) to a vacuum state  $|0\rangle$ . Even though the coherent state is a quantum state, it can be considered as a classical state because the dynamics of its quadratures is described by Maxwell equations, among other reasons [9].

Once the state is prepared in the lab, the next step is to make it interact with the environment and the object. We model this interaction by using a beam splitter of low reflectivity, since the target is expected to be hard to detect, i.e. to show low reflectivity. In this step, the signal is mixed with the environment, which is described by a thermal state (Eq. 1.12). In the case of a highly noisy environment, our signal is surrounded by a large amount of thermal photons ( $n_{th} = \lambda/(1 - \lambda) \gg 1$ ).

Then, we will rewrite Eq. 1.20 for our problem. Let us consider as incoming states the signal ( $\hat{a}$ ) and the environment ( $\hat{a}_{th}$ ). Among the outgoing beams, only one of them is accessible, the one corresponding to the reflection of the signal and the transmission of the thermal state ( $\hat{b}$ ). Its annihilation operator is represented as  $\hat{b}$ . The relation between annihilation operators is

$$\hat{b} = r\hat{a} + t\hat{a}_{th} = \sqrt{\eta}\hat{a} + \sqrt{1 - \eta}\hat{a}_{th}, \quad (2.3)$$



where  $\eta$  is the reflectivity ( $\eta = |r|^2 = 1 - |t|^2$ ).

Finally, we have to choose the observable for the measurement. Needless to say that we aim at obtaining the maximum quantity of information from the system. In the classical case, the measurement corresponds to the expectation value of the quadrature  $\hat{x} = \frac{1}{2}(\hat{b} + \hat{b}^\dagger)$  [10].

As we can work in both the Schrödinger and the Heisenberg pictures, we will apply the change produced by the beam splitter (Eq. 2.3) to the operator  $\hat{x}$  instead of to  $|\alpha\rangle$  for convenience. The operator results in

$$\hat{x} = \frac{1}{2}(\sqrt{\eta}(\hat{a} + \hat{a}^\dagger) + \sqrt{1-\eta}(\hat{a}_{\text{th}} + \hat{a}_{\text{th}}^\dagger)), \quad (2.4)$$

where  $\hat{a}$  and  $\hat{a}^\dagger$  act on the coherent state and  $\hat{a}_{\text{th}}$  and  $\hat{a}_{\text{th}}^\dagger$  on the thermal state.

In order to obtain the SNR, we need to calculate the expectation value of the quadrature  $\hat{x}$  and of  $\hat{x}^2$ . For the calculation of  $\langle \hat{x} \rangle$ , the following quantities are needed:

- $\langle \hat{a} \rangle = \langle \alpha | \hat{a} | \alpha \rangle = \alpha$
- $\langle \hat{a}^\dagger \rangle = \langle \alpha | \hat{a}^\dagger | \alpha \rangle = \alpha^*$
- $\langle \hat{a}^\dagger \hat{a} \rangle = \langle \alpha | \hat{a}^\dagger \hat{a} | \alpha \rangle = |\alpha|^2$ .
- $\langle \hat{a}_{\text{th}} \rangle = \langle \hat{a}_{\text{th}}^\dagger \rangle^* = \text{Tr}(\hat{a}_{\text{th}} \hat{\rho}_{\text{th}}) = \text{Tr} \left( (1-\lambda) \sum_{n=0}^{\infty} \lambda^n \hat{a}_{\text{th}} |n\rangle \langle n| \right)$ .  
 $= \text{Tr} \left( (1-\lambda) \sum_{n=0}^{\infty} \lambda^n \sqrt{n} |n-1\rangle \langle n| \right) = 0$ .

where  $|\alpha\rangle$  is the coherent state (Eq. 2.2) and  $\hat{\rho}_{\text{th}}$  is the thermal density matrix (Eq. 1.12). Replacing the obtained results in  $\langle \hat{x} \rangle$ , we obtain

$$\langle \hat{x} \rangle = \frac{\sqrt{\eta}}{2}(\alpha + \alpha^*) = \sqrt{\eta}\alpha = \sqrt{\eta N}, \quad (2.5)$$

where we have assumed without loss of generality that  $\alpha \in \mathfrak{R}$ .  $N = |\alpha|^2$  is the expected number of photons of the coherent state.

For the calculation of  $\langle \hat{x}^2 \rangle$ , we need to obtain different quantities comprising products of the operators  $\hat{a}$ ,  $\hat{a}^\dagger$ ,  $\hat{a}_{\text{th}}$  and  $\hat{a}_{\text{th}}^\dagger$ . We can see that the mean value of any product of operators containing an odd number of operators in the thermal Hilbert space is 0, which simplifies the calculation. Let us now add the remaining results:

- $\langle \hat{a}^2 \rangle = \langle \alpha | \hat{a} \hat{a} | \alpha \rangle = \alpha^2$ .
- $\langle \hat{a}^{\dagger 2} \rangle = \langle \alpha | \hat{a}^\dagger \hat{a}^\dagger | \alpha \rangle = \alpha^{*2}$ .

- $\langle \hat{a}\hat{a}^\dagger \rangle = \langle \alpha | (\hat{a}^\dagger \hat{a} + 1) | \alpha \rangle = |\alpha|^2 + 1.$
- $\langle \hat{a}_{\text{th}}^\dagger \hat{a}_{\text{th}} \rangle = \text{Tr}(\hat{a}_{\text{th}}^\dagger \hat{a}_{\text{th}} \hat{\rho}_{\text{th}}) = \text{Tr}\left((1 - \lambda) \sum_{n=0}^{\infty} \lambda^n \hat{a}_{\text{th}}^\dagger \hat{a}_{\text{th}} |n\rangle\langle n|\right)$   
 $= \text{Tr}\left((1 - \lambda) \sum_{n=0}^{\infty} \lambda^n n |n\rangle\langle n|\right)$   
 $= (1 - \lambda) \lambda \sum_{n=0}^{\infty} n \lambda^{n-1} = \lambda(1 - \lambda) \sum_{n=0}^{\infty} \frac{\partial}{\partial \lambda} \lambda^n$   
 $= \lambda(1 - \lambda) \frac{\partial}{\partial \lambda} \frac{1}{1 - \lambda} = \frac{\lambda}{1 - \lambda} = n_{\text{th}}.$
- $\langle \hat{a}_{\text{th}} \hat{a}_{\text{th}}^\dagger \rangle = \text{Tr}(\hat{a}_{\text{th}} \hat{a}_{\text{th}}^\dagger \hat{\rho}_{\text{th}}) = \text{Tr}(\hat{\rho}_{\text{th}} (\hat{a}_{\text{th}}^\dagger \hat{a}_{\text{th}} + 1)) = n_{\text{th}} + 1.$

By considering again  $\alpha \in \Re$ ,  $\langle \hat{x}^2 \rangle$  is given by

$$\begin{aligned} \langle \hat{x}^2 \rangle &= \frac{1}{4}(\eta(\langle \hat{a}^2 \rangle + \langle \hat{a}^{\dagger 2} \rangle) + \langle \hat{a}^\dagger \hat{a} \rangle + \langle \hat{a} \hat{a}^\dagger \rangle) + (1 - \eta)(\langle \hat{a}_{\text{th}}^\dagger \hat{a}_{\text{th}} \rangle + \langle \hat{a}_{\text{th}} \hat{a}_{\text{th}}^\dagger \rangle) \\ &= \frac{1}{4}(\eta(4\alpha^2 + 1) + (1 - \eta)(2n_{\text{th}} + 1)) \\ &= \eta(N + 1/4) + \frac{1}{2}(1 - \eta)(n_{\text{th}} + 1/2). \end{aligned} \quad (2.6)$$

Finally, we can calculate the SNR for the classical protocol by replacing Eqs. 2.5 and 2.6 in Eq. 2.1,

$$\text{SNR}_{\text{C}} = \frac{\langle x \rangle^2}{\langle x^2 \rangle - \langle x \rangle^2} = \frac{2N\eta}{(1 - \eta)n_{\text{th}} + 1/2}. \quad (2.7)$$

## 2.2 Quantum Protocol

Let us now analyse the quantum protocol to afterwards compare it with the classical one. The main steps are the same: quantum state preparation, interaction and measurement. The key difference between both protocols is the use of entangled states, as described below. A schematic view of the whole quantum illumination protocol is depicted in Fig. 2.2.

Instead of using a coherent state, our resource for the quantum protocol is the two-mode squeezed state (TMSS), since it offers an optimal performance and the experimental generation is simple [10]. Its general form is

$$|\xi_{1,2}\rangle = e^{-\xi \hat{a}_1^\dagger \hat{a}_2^\dagger + \xi^* \hat{a}_1 \hat{a}_2} |0_1, 0_2\rangle = \text{sech}(r) \sum_{n=0}^{\infty} [-e^{i\phi} \tanh(r)]^n |n_1, n_2\rangle, \quad (2.8)$$

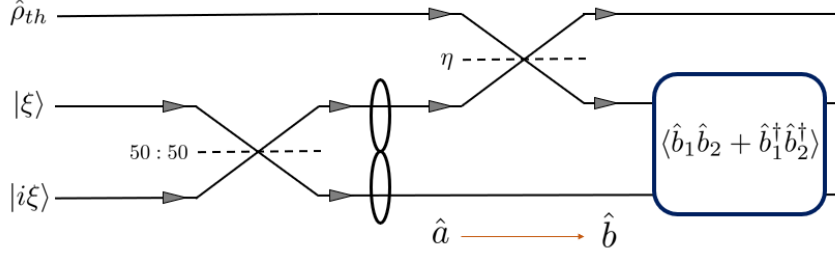


Figure 2.2: **Scheme of the quantum illumination protocol.** First, two vacuum states squeezed in orthogonal directions are mixed through a 50:50 beam splitter. This results in a two-mode squeezed state (TMSS) (Eq. 2.9). Then, one of the entangled modes (signal beam) is mixed with a thermal state through a low reflectivity beam splitter, simulating the interaction. The other one (idler beam) is kept in the lab. Finally, a joint measurement,  $\hat{b}_1 \hat{b}_2 + \hat{b}_1^\dagger \hat{b}_2^\dagger$ , is realized, where 1 and 2 refer to each of the beams. The orange arrow represents the change produced by the beam splitter on the fields (Eq. 2.3), represented by their respective annihilation operators. The subindexes 1 and 2 correspond to the signal and idler modes respectively.

where  $r = |\xi|$  and  $\phi = \text{Arg}(\xi)$ . In particular, we chose one experimentally generated by mixing two squeezed vacuum states  $|\xi_1\rangle$  and  $|\xi_2\rangle$  with a 50:50 beam splitter, i.e. with the same reflection and transmission coefficients, where  $\xi_1$  and  $\xi_2$  have the same modulus ( $r_1 = r_2$ ) and are squeezed in perpendicular directions ( $\phi_2 - \phi_1 = \pi/2$ ). The global phase  $\phi$  can be set to  $-\pi$  without loss of generality, so the state results in

$$|\lambda_{12}\rangle = \sqrt{1 - \lambda^2} \sum_{n=0}^{\infty} \lambda^n |n, n\rangle, \quad (2.9)$$

where  $\lambda = \tanh(r)$  is a real positive parameter smaller than 1. Once the state is prepared, one of the modes, that we call "signal" ( $\hat{a}_1$ ), is sent towards the object, whereas the other entangled mode, known as "idler" ( $\hat{a}_2$ ), is kept in the laboratory. The interaction with the object is once again modelled by a low reflectivity beam splitter, exactly as in the classical protocol. The generated transformation is the same that the one given by Eq. 2.3, but replacing  $\hat{a}$  by  $\hat{a}_1$ , to make it clear that it acts on the signal mode.

Finally, we need to choose an observable to measure and obtain the SNR of the quantum protocol. The measurement providing us the most information about the reflectivity,  $\eta$ , is the expectation value of  $\hat{x}_1 \hat{x}_2 - \hat{p}_1 \hat{p}_2 = \hat{b}_1 \hat{b}_2 + \hat{b}_1^\dagger \hat{b}_2^\dagger$  [10], where  $\hat{b}$  represents an annihilation operator after the interaction with the object, and the subindexes 1 and 2 correspond to the signal and idler modes respectively.

In the case of the mode 1 (signal), it suffers the transformation held by Eq. 2.3. On the other hand, the idler mode is not changed at all, so  $\hat{b}_2 = \hat{a}_2$ . Applying these two transformations to the desired observable, we express it in terms of the annihilation operators of the initial states:

$$\begin{aligned}\hat{b}_1\hat{b}_2 + \hat{b}_1^\dagger\hat{b}_2^\dagger &= (\sqrt{\eta}\hat{a}_1 + \sqrt{1-\eta}\hat{a}_{\text{th}})\hat{a}_2 + (\sqrt{\eta}\hat{a}_1^\dagger + \sqrt{1-\eta}\hat{a}_{\text{th}}^\dagger)\hat{a}_2^\dagger \\ &= \sqrt{\eta}(\hat{a}_1\hat{a}_2 + \hat{a}_1^\dagger\hat{a}_2^\dagger) + \sqrt{1-\eta}(\hat{a}_{\text{th}}\hat{a}_2 + \hat{a}_{\text{th}}^\dagger\hat{a}_2^\dagger).\end{aligned}\quad (2.10)$$

For the calculation of the expectation value of Eq. 2.10, we will use again that the expectation value of a thermal annihilation or creation operator is 0. Below, different needed calculations are shown:

- $\langle \hat{a}_1^\dagger \hat{a}_1 \rangle = \langle \hat{a}_2^\dagger \hat{a}_2 \rangle = \langle \lambda_{12} | \hat{a}_1^\dagger \hat{a}_1 | \lambda_{12} \rangle$ 

$$\begin{aligned}&= (1-\lambda^2) \sum_{m=0}^{\infty} \lambda^m \langle m, m | \hat{a}_1^\dagger \hat{a}_1 \sum_{n=0}^{\infty} \lambda^n |n, n\rangle \\ &= (1-\lambda^2) \sum_{n=0}^{\infty} n \lambda^{2n} = \lambda^2 (1-\lambda^2) \sum_{n=0}^{\infty} \frac{\partial}{\partial \lambda^2} \lambda^{2n} \\ &= \lambda^2 (1-\lambda^2) \frac{\partial}{\partial \lambda^2} \frac{1}{1-\lambda^2} = \frac{\lambda^2}{1-\lambda^2} = N.\end{aligned}$$
- $\langle \hat{a}_1 \hat{a}_2 \rangle = \langle \hat{a}_1^\dagger \hat{a}_2^\dagger \rangle^* = (1-\lambda^2) \sum_{m=0}^{\infty} \lambda^m \langle m, m | \hat{a}_1 \hat{a}_2 \sum_{n=0}^{\infty} \lambda^n |n, n\rangle$ 

$$\begin{aligned}&= (1-\lambda^2) \sum_{m=0}^{\infty} \lambda^m \langle m, m | \sum_{n=1}^{\infty} n \lambda^n |n-1, n-1\rangle \\ &= \lambda (1-\lambda^2) \sum_{n=0}^{\infty} \lambda^{2n} (n+1) = \frac{\lambda}{1-\lambda^2} = \sqrt{N(N+1)}.\end{aligned}$$

Replacing these expressions in the expectation value of Eq. 2.10, we obtain

$$\langle \hat{b}_1 \hat{b}_2 + \hat{b}_1^\dagger \hat{b}_2^\dagger \rangle = 2\sqrt{\eta N(N+1)}.\quad (2.11)$$

Notice that, in this case,  $N$  is the number of photons both of the idler and the signal beams, and it is given by the parameter  $\lambda$  of the TMSS.

Similarly to the classical protocol, we also have to find  $\langle (\hat{b}_1 \hat{b}_2 + \hat{b}_1^\dagger \hat{b}_2^\dagger)^2 \rangle$ . For this goal, we will divide again the calculation into:

- $\langle \hat{a}_1^2 \hat{a}_2^2 \rangle = \langle \hat{a}_1^{\dagger 2} \hat{a}_2^{\dagger 2} \rangle^* = (1-\lambda^2) \sum_{m=0}^{\infty} \lambda^m \langle m, m | \sum_{n=2}^{\infty} n(n-1) \lambda^n |n-2, n-2\rangle$ 

$$\begin{aligned}&= (1-\lambda^2) \sum_{m=0}^{\infty} \lambda^m \langle m, m | \sum_{k=0}^{\infty} (k+2)(k+1) \lambda^{k+2} |k, k\rangle \\ &= (1-\lambda^2) \sum_{n=0}^{\infty} \lambda^{2(n+1)} (n+1)(n+2) = \lambda^2 (1-\lambda^2) \sum_{n=0}^{\infty} \frac{\partial^2}{(\partial \lambda^2)^2} \lambda^{2(n+2)} \\ &= \lambda^2 (1-\lambda^2) \frac{\partial^2}{(\partial \lambda^2)^2} \frac{\lambda^2}{1-\lambda^2} = 2 \left[ \frac{\lambda}{1-\lambda^2} \right]^2 = 2N(N+1).\end{aligned}$$

$$\begin{aligned}
\bullet \langle \hat{a}_1^\dagger \hat{a}_1 \hat{a}_2^\dagger \hat{a}_2 \rangle &= (1-\lambda^2) \sum_{m=0}^{\infty} \lambda^m \langle m, m | \sum_{n=0}^{\infty} n^2 \lambda^n |n, n\rangle = (1-\lambda^2) \sum_{n=0}^{\infty} \lambda^{2n} n^2 \\
&= (1-\lambda^2) \left[ \lambda^4 \sum_{n=0}^{\infty} n(n-1) \lambda^{2(n-2)} + \lambda^2 \sum_{n=0}^{\infty} n \lambda^{2(n-1)} \right] \\
&= \lambda^2 (1-\lambda^2) \left[ \lambda^2 \frac{\partial^2}{(\partial \lambda^2)^2} \frac{1}{1-\lambda^2} + \frac{\partial}{\partial \lambda^2} \frac{1}{1-\lambda^2} \right] = \\
&= \frac{\lambda^2}{1-\lambda^2} \left[ 2 \frac{\lambda^2}{1-\lambda^2} + 1 \right] = N(2N+1).
\end{aligned}$$

Now we can compute  $\langle (\hat{b}_1 \hat{b}_2 + \hat{b}_1^\dagger \hat{b}_2^\dagger)^2 \rangle$ ,

$$\begin{aligned}
\langle (\hat{b}_1 \hat{b}_2 + \hat{b}_1^\dagger \hat{b}_2^\dagger)^2 \rangle &= \langle (\sqrt{\eta} (\hat{a}_1 \hat{a}_2 + \hat{a}_1^\dagger \hat{a}_2^\dagger) + \sqrt{1-\eta} (\hat{a}_{\text{th}} \hat{a}_2 + \hat{a}_{\text{th}}^\dagger \hat{a}_2^\dagger))^2 \rangle \\
&= \eta (\langle \hat{a}_1^2 \hat{a}_2^2 \rangle + \langle \hat{a}_1^{\dagger 2} \hat{a}_2^{\dagger 2} \rangle) + 2 \langle \hat{n}_1 \hat{n}_2 \rangle + \langle \hat{n}_1 \rangle + \langle \hat{n}_2 \rangle + 1 + \\
&\quad (1-\eta) (2 \langle \hat{n}_{\text{th}} \hat{n}_2 \rangle + \langle \hat{n}_{\text{th}} \rangle + \langle \hat{n}_2 \rangle + 1) \\
&= \eta (6N^2 + 7N + 1) + (1-\eta) (2Nn_{\text{th}} + N + n_{\text{th}} + 1). \quad (2.12)
\end{aligned}$$

Therefore, the quantum SNR is easily calculated by replacing Eqs. 2.11 and 2.12 in Eq. 2.1:

$$\text{SNR}_Q = \frac{4\eta N(N+1)}{\eta(2N(N-n_{\text{th}}+1) - n_{\text{th}}) + 2Nn_{\text{th}} + N + n_{\text{th}} + 1}. \quad (2.13)$$

## 2.3 Comparison

Finally, in this Section, we will compare the classical and quantum SNR. For the sake of fairness in the comparison, we will consider the same number of signal photons ( $N$ ) in both cases. We are interested in the region of parameters where the performance of the quantum protocol overcomes the classical one,  $\text{SNR}_Q > \text{SNR}_C$ . This can be expressed with the condition

$$\frac{\text{SNR}_Q}{\text{SNR}_C} = \frac{(N+1)(2n_{\text{th}}(1-\eta) + 1)}{(N+1)(2\eta N + 1) + (1-\eta)(2N+1)n_{\text{th}}} > 1. \quad (2.14)$$

Analysing this relation, we notice that in the limit  $N \gg 1$ , the quantum protocol does not offer any improvement. All this can also be observed in Fig. 2.3. Solving the inequality for  $N$ , we get that it holds when

$$N^2 + N - \frac{1-\eta}{2\eta} n_{\text{th}} < 0. \quad (2.15)$$

This equation is a parabola and it describes the crossing between surfaces observed in Fig. 2.3. As it is convex, we are interested in the region between

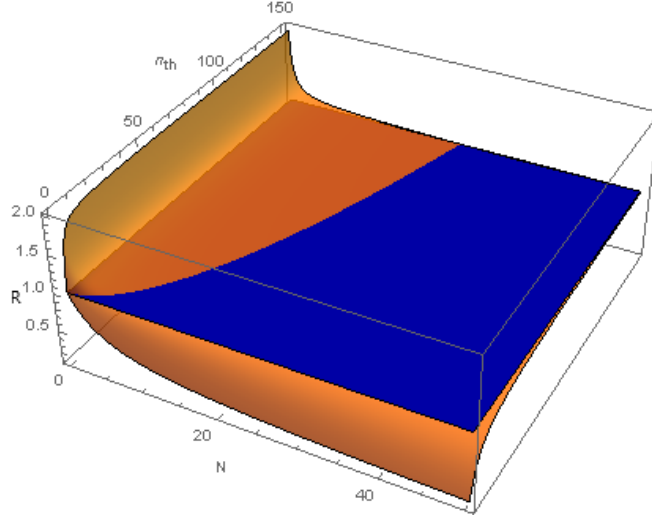


Figure 2.3: **Representation of the inequality given by Eq. 2.14 ( $R$ ) in terms of the signal photons ( $N$ ) and the thermal ones ( $n_{\text{th}}$ ).** The orange surface represents the ratio between the quantum and classical protocols for a low reflectivity value ( $\eta = 0.1$ ) and the blue surface represents the value 1 as a reference. The quantum protocol gives better resolution when the orange surface is above the blue one.

its roots. Given that  $N$  must be positive, we find that there is always a region of  $N$  in which the quantum protocol improves the classical one,

$$0 < N < \frac{-1 + \sqrt{1 + 2n_{\text{th}} \frac{1-\eta}{\eta}}}{2}, \quad (2.16)$$

which is always positive, since  $\frac{1-\eta}{\eta} \geq 0 \forall \eta$ , and  $n_{\text{th}}$  is also a positive parameter. The maximum advantage is achieved in the limit  $N \ll 1$  and in a very noisy environment,  $n_{\text{th}} \gg 1$ . Computing the limit of Eq. 2.14 when  $n_{\text{th}} \rightarrow \infty$  and  $N \rightarrow 0$ , we obtain that the gain given by the quantum protocol over the classical is a factor of 2.

The physical interpretation of this result is that a quantum protocol can overcome the performance of the optimal classical one when the signal is weak in comparison with the thermal noise.

## 2.4 Quantum Radar

A quantum radar is a detection technology based on quantum illumination. It can be understood as a generalization, since quantum illumination consists in deciding whether an object is or not in a particular point in space, whereas in the quantum radar problem we do not know the position of the object a priori.

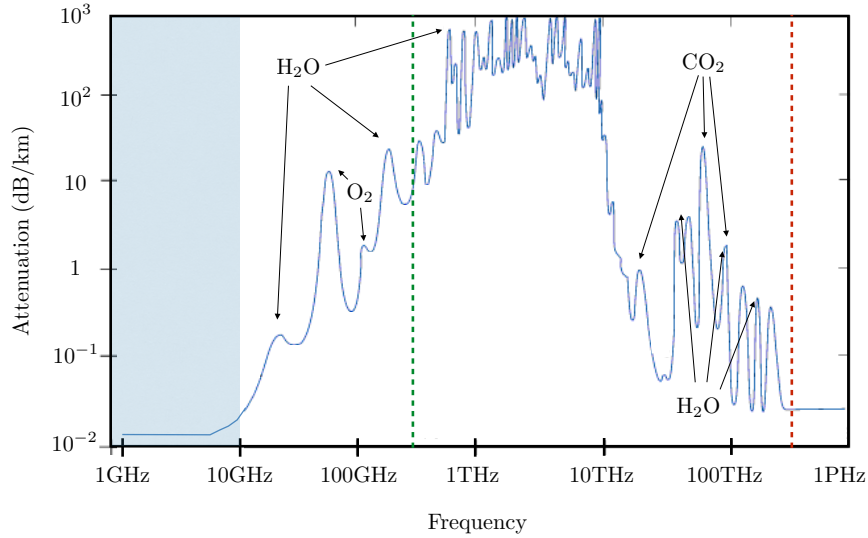


Figure 2.4: **Attenuation caused by the atmosphere (dB/km) as a function of the frequency** [11]. The blue area correspond to the frequencies of propagating quantum microwaves. The green line separates microwaves from infrared, and the red line, infrared from visible frequencies.

The difference between the conventional radar and the quantum one would be the amount of resources in terms of photons needed to detect the object with a certain probability. The classical radar uses light to enhance its sensitivity, while the quantum radar uses entanglement to reduce the signal photons. This would be useful, for example, in case that we do not want that the "enemy" aircraft knows that we are detecting it or when we want to detect a stealth aircraft, specifically designed to reflect a low amount of photons.

In order to detect an object with photons, the wavelength of the radiation used to detect it must be of the same order as the size of the target. This implies that the photons sent must be in the microwave regime, because its wavelength is of the order of centimetres. Besides, the atmosphere is almost transparent for microwaves (See Fig. 2.4), which also supports the use of microwaves for radar detection. Nevertheless, the manipulation of the beams and measurement can be done both in the microwave and the optical regimes. Let us now briefly describe the advantages and disadvantages of using each frequency.

### 2.4.1 Optical vs Microwave Regime

Due to the fact that it is essential to utilize microwaves in the target detection, it is a clear candidate to be used in quantum radar. The reason for thinking in using photons in the optical regime is because of the already

developed technology for this frequency range. In particular, the existence of efficient photodetectors of single photons, currently under development in the microwave regime, is the main reason for developing this technology for the optical range.

Nowadays, strong efforts are performed to create an efficient photodetector in microwaves. This would avoid microwave-to-optical photon transducers. The fact of not having to transform the frequency of the signal could considerably raise the overall detection efficiency.



## Chapter 3

# Photon Subtraction

Gaussian states are particularly convenient for quantum illumination, due to their experimental feasibility, their resilience and relatively straightforward theoretical description and manipulation. Nevertheless, non-Gaussian states have been studied in the framework of quantum information, demonstrating that a stronger entanglement can be achieved compared to Gaussian states [2]. This fact makes them look promising candidates to overcome the performance of protocols based on Gaussian quantum states, but we have to keep in mind that higher entanglement does not necessarily mean better results [10].

One of the main methods for transforming a Gaussian state into a non-Gaussian one is known as photon subtraction (PS). It consists in applying an annihilation operator  $\hat{a}$  to our Gaussian state. This technique is employed for other various purposes, such as the creation of cat states (a superposition of two coherent states)[12].

Notice that, despite its name, the mean number of photons after the photon subtraction may be equal or greater than before. This fact can be straightforwardly appreciated in a coherent state; as it is an eigenvector of the annihilation operator, the number of photons is the same. This fact turns out to be key in quantum illumination, since two different protocols, with different signal states, must be always compared by fixing the same number of resources in terms of photons for both protocols.

In this Chapter, we will study the effect of the photon subtraction operation (PS) in a quantum illumination protocol. Firstly, in Section 3.1, we compare the performances of the already seen TMSS with and without PS. We prove that the PS protocol does not improve the Gaussian protocol so, in Section 3.2, we consider an arbitrary single-mode Gaussian state and study how photon subtraction affects the number of photons. We obtain a family of Gaussian states for which the number of photon maximally decreases. Finally, in Section 3.3, we generate a particular two-mode Gaussian state that, after tracing out the idler mode, results in a single-mode Gaussian state

that belongs to the family of Gaussian states found in the previous Section. Then, the SNR is calculated and compared with the Gaussian protocol, in order to determine whether photon subtraction improves the result.

### 3.1 PS on a Two-Mode Squeezed State

It is known that non-Gaussian states show higher computational power in continuous variable quantum computing than Gaussian states. A logical question consequently arisen is whether we can improve the results shown by the quantum illumination protocol developed in Section 2.2 with squeezed states by employing photon subtraction. In this Section, we are going to compute the SNR of the new quantum protocol and compare it with Eq. 2.13.

For the sake of simplicity, we will apply the annihilation operator only to the signal beam, and not to the idler one, i.e. to the mode 1 of Eq. 2.9. This results in the state

$$|\lambda_{\text{PS}}\rangle = \frac{\hat{a}_1 |\lambda_{12}\rangle}{\langle \lambda_{12} | \hat{a}_1^\dagger \hat{a}_1 | \lambda_{12} \rangle} = \frac{1 - \lambda^2}{\lambda} \sum_{n=0}^{\infty} \lambda^n \sqrt{n} |n-1, n\rangle, \quad (3.1)$$

which has been normalized. The measured operator will be the one of Eq. 2.10, the same as for the previous quantum protocol. We divide again the calculation of the expectation value in parts, presenting the results below,

$$\begin{aligned} \bullet \langle \hat{a}_1 \hat{a}_2 \rangle_{\text{PS}} &= \frac{(1 - \lambda^2)^2}{\lambda^2} \sum_{m=0}^{\infty} \sum_{n=1}^{\infty} \lambda^m \lambda^n n \sqrt{n-1} \sqrt{m} \delta_{m-1, n-2} \delta_{m, n-1} \\ &= \frac{(1 - \lambda^2)^2}{\lambda^2} \sum_{m=0}^{\infty} \sum_{k=0}^{\infty} \lambda^m \lambda^{k+1} (k+1) \sqrt{k} \sqrt{m} \delta_{m, k} \\ &= \lambda (1 - \lambda^2)^2 \sum_{n=0}^{\infty} \lambda^{2(n-1)} n (n+1) = \\ &= \lambda (1 - \lambda^2)^2 \frac{\lambda^2}{1 - \lambda^2} = 2 \frac{\lambda}{1 - \lambda^2} = 2 \sqrt{N'(N'+1)} = \langle \hat{a}_1^\dagger \hat{a}_2^\dagger \rangle_{\text{PS}}^* \end{aligned}$$

where  $N'$  is the mean number of photons defined for the TMSS without photon subtraction.  $N$  is used for the number of photons of the signal mode of each protocol. Now, we replace the addends in the expectation value of the operator, obtaining the expression

$$\langle \hat{b}_1 \hat{b}_2 + \hat{b}_1^\dagger \hat{b}_2^\dagger \rangle_{\text{PS}} = 4 \sqrt{\eta N'(N'+1)}. \quad (3.2)$$

We follow the same process than for the previous protocols, calculating the expectation value of the operator squared:

- $\langle \hat{a}_1^\dagger \hat{a}_1 \rangle_{\text{PS}} = \frac{\langle \hat{a}_1^\dagger \hat{a}_1^\dagger \hat{a}_1 \hat{a}_1 \rangle}{\langle \hat{a}_1^\dagger \hat{a}_1 \rangle} = \frac{\langle \hat{a}_1^\dagger \hat{a}_1 \hat{a}_1^\dagger \hat{a}_1 \rangle - \langle \hat{a}_1^\dagger \hat{a}_1 \rangle}{\langle \hat{a}_1^\dagger \hat{a}_1 \rangle}$   
 $= \frac{N'(2N' + 1) - N'}{N'} = 2N' = N$
- $\langle \hat{a}_2^\dagger \hat{a}_2 \rangle_{\text{PS}} = \frac{\langle \hat{a}_1^\dagger \hat{a}_1 \hat{a}_2^\dagger \hat{a}_2 \rangle}{\langle \hat{a}_1^\dagger \hat{a}_1 \rangle} = \frac{N'(2N' + 1)}{N'} = 2N' + 1$
- $\langle \hat{a}_1^2 \hat{a}_2^2 \rangle_{\text{PS}} = \frac{(1 - \lambda^2)^2}{\lambda^2} \sum_{m=0}^{\infty} \sum_{n=2}^{\infty} \lambda^{m+n} \sqrt{nm} (n-1)(n-2) \delta_{m-1, n-3} \delta_{m, n-2}$   
 $= \frac{(1 - \lambda^2)^2}{\lambda^2} \sum_{n=0}^{\infty} \lambda^{2n+2} n(n+1)(n+2)$   
 $= \frac{(1 - \lambda^2)^2}{\lambda^2} \lambda^4 \sum_{n=0}^{\infty} \frac{\partial^3}{(\partial \lambda^2)^3} (\lambda^2)^{n+2}$   
 $= (1 - \lambda^2)^2 \lambda^2 \frac{\partial^3}{(\partial \lambda^2)^3} \frac{\lambda^4}{1 - \lambda^2} = 6 \frac{\lambda^2}{(1 - \lambda^2)^2} = 6N'(N' + 1)$
- $\langle \hat{a}_1^\dagger \hat{a}_1 \hat{a}_2^\dagger \hat{a}_2 \rangle_{\text{PS}} = \frac{(1 - \lambda^2)^2}{\lambda^2} \sum_{m=0}^{\infty} \lambda^m \langle m, m | \sum_{n=0}^{\infty} \lambda^n n^2 (n-1) |n, n\rangle$   
 $= \frac{(1 - \lambda^2)^2}{\lambda^2} \sum_{n=0}^{\infty} \lambda^{2n} n^2 (n-1)$   
 $= \frac{(1 - \lambda^2)^2}{\lambda^2} \left[ \sum_{n=0}^{\infty} n(n-1)(n-2) \lambda^{2n} + 2 \sum_{n=0}^{\infty} n(n-1) \lambda^{2n} \right]$   
 $= \lambda^2 (1 - \lambda^2)^2 \left[ 6 \frac{\lambda^2}{(1 - \lambda^2)^4} + 4 \frac{1}{(1 - \lambda^2)^3} \right] = 2N'(3N' + 2)$

In order to calculate the expected number of photons of both modes, 1 and 2, we have used results obtained for the TMSS, which are not labelled with the subindex PS (photon subtraction). The obtained result for  $\langle \hat{a}_1^\dagger \hat{a}_1 \rangle_{\text{PS}}$  is of the greatest importance, since it shows that photon subtraction has doubled the number of photons with respect to the TMSS. The expression for  $\langle (\hat{b}_1 \hat{b}_2 + \hat{b}_1^\dagger \hat{b}_2^\dagger)^2 \rangle_{\text{PS}}$  is

$$\begin{aligned} \langle (\hat{b}_1 \hat{b}_2 + \hat{b}_1^\dagger \hat{b}_2^\dagger)^2 \rangle_{\text{PS}} &= \langle (\sqrt{\eta} (\hat{a}_1 \hat{a}_2 + \hat{a}_1^\dagger \hat{a}_2^\dagger) + \sqrt{1 - \eta} (\hat{a}_{\text{th}} \hat{a}_2 + \hat{a}_{\text{th}}^\dagger \hat{a}_2^\dagger))^2 \rangle \\ &= 2\eta (12N'^2 + 12N' + 1) + (1 - \eta)(2N' + (4N' + 3)n_{\text{th}} + 2). \end{aligned} \quad (3.3)$$

Substituting Eqs. 3.2 and 3.3 in Eq. 2.1, we obtain an expression for the SNR of this protocol,

$$\begin{aligned} \text{SNR}_{\text{PS}} &= \frac{16\eta N'(N'+1)}{2(N'+1) + (4N'+3)(2\eta N' - \eta n_{\text{th}} + n_{\text{th}})} \\ &= \frac{4\eta N(N+2)}{N + (2N+3)(\eta N - \eta n_{\text{th}} + n_{\text{th}}) + 2}, \end{aligned} \quad (3.4)$$

In the first equality, the SNR depends on the number of photons of a TMSS ( $N'$ ). Since we want the SNR to depend on the number of photons of the signal ( $N$ ), we have made the change  $N' = N/2$ . This is done to be able to compare both protocols employing the same number of photons.

Finally, the comparison between Gaussian and non-Gaussian protocols is performed via SNR, and is given by

$$\frac{\text{SNR}_{\text{PS}}}{\text{SNR}_{\text{Q}}} = \frac{(N+2)(2\eta(N+1)N + N - (\eta-1)(2N+1)n_{\text{th}} + 1)}{(N+1)(N + (2N+3)(\eta N - \eta n_{\text{th}} + n_{\text{th}}) + 2)}, \quad (3.5)$$

and represented in Fig. 3.1. There is a region of parameters for which the non-Gaussian protocol gives a better performance than the Gaussian one. Specifically, for  $n_{\text{th}} = 0$  thermal photons, the ratio reaches a maximum value of  $1 + \frac{\eta}{1+4\sqrt{\eta}+3\eta}$  for  $N = \eta^{-1/2}$  expected signal photons. This fact may seem relevant but, comparing with Fig. 2.3, we see that the PS protocol is better than the one without it only in a region where both are worse than the classical protocol. We can understand this by observing Fig. 3.2, where we have compared both the quantum Gaussian protocol and the PS one with the classical protocol. We observe that, even though the non-Gaussian protocol overcomes the classical one for small values of  $N$ , the Gaussian protocol is still better in the region of interest. This lets us conclude that the PS state of Eq. 3.1 performs worse than the TMSS of Eq. 2.9, even though the former could show a stronger entanglement.

## 3.2 PS on Single-Mode Gaussian States

In the previous Section we have observed that, far from reducing the number of photons, photon subtraction doubles it for a two-mode squeezed state, making the non-Gaussian state useless for our purpose. In this Section, we address the question whether this technique also increases the number of photons for a general single-mode Gaussian state (Eq. 1.16). This is relevant since, if we trace out the idle of an arbitrary two-mode Gaussian state, the reduced density matrix of the signal is a single-mode Gaussian state. We will see that this is not generally true, and find the relation between squeezing and displacement that achieves the largest reduction in the number of photons.

The quantity we want to compute is the difference between the expectation number of photons of a general Gaussian state before and after applying an annihilation operator, which are expressed by

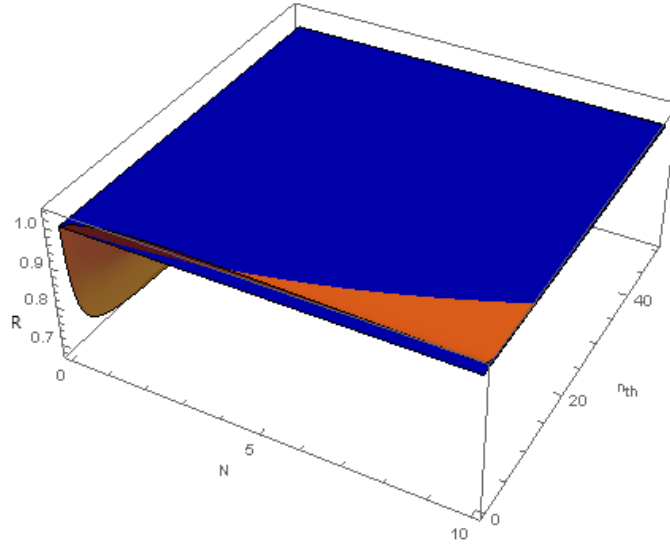


Figure 3.1: Representation of the ratio between quantum protocols' SNRs with and without photon subtraction ( $R$ ), given by Eq. 3.5 (orange surface), in terms of the signal and thermal photons ( $N$  and  $n_{th}$  respectively) for a reflectivity value of  $\eta = 0.1$ . The blue surface value is 1, and serves as a reference. The photon subtraction protocol (non-Gaussian) gives better performance than the Gaussian one when the orange surface is above the blue one.

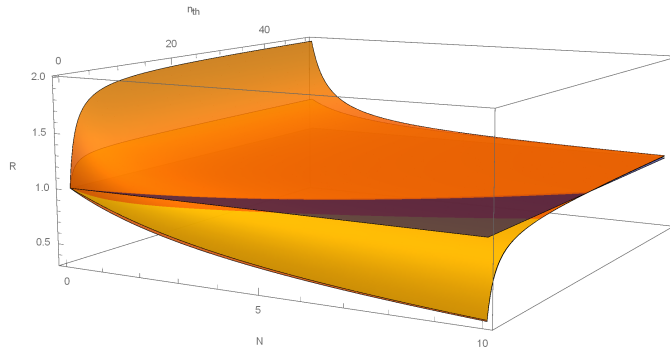


Figure 3.2: Representation of the ratio between the quantum Gaussian protocol and the classical protocol (orange surface) and the ratio between the PS protocol and the classical protocol (yellow surface), in terms of the signal photons ( $N$ ) and thermal photons ( $n_{th}$ ). The blue surface serves as a reference, and takes the value 1. The quantum protocols give better performance than the classical one when their respective surfaces lie above the blue one.

$$N_{\text{Gauss}} = \text{Tr}\left(\hat{a}^\dagger \hat{a} \hat{D}(\alpha) \hat{S}(\xi) \hat{\rho}_{\text{th}} \hat{S}^\dagger(\xi) \hat{D}^\dagger(\alpha)\right), \quad (3.6)$$

$$N_{\text{PS}} = \frac{\text{Tr}\left(\hat{a}^\dagger \hat{a} \hat{a} \hat{D}(\alpha) \hat{S}(\xi) \hat{\rho}_{\text{th}} \hat{S}^\dagger(\xi) \hat{D}^\dagger(\alpha) \hat{a}^\dagger\right)}{\text{Tr}\left(\hat{a} \hat{D}(\alpha) \hat{S}(\xi) \hat{\rho}_{\text{th}} \hat{S}^\dagger(\xi) \hat{D}^\dagger(\alpha) \hat{a}^\dagger\right)} \quad (3.7)$$

respectively, where the denominator of the second formula comes from the normalization process.

In order to calculate these expressions, we need the commutation relations between the displacement and squeezing operators (Eqs. 1.14 and 1.15) and the ladder operators. The relation between the operators obeys the equations

$$\hat{a} \hat{D}(\alpha) = \hat{D}(\alpha) (\hat{a} + \alpha), \quad \hat{a}^\dagger \hat{D}(\alpha) = \hat{D}(\alpha) (\hat{a}^\dagger + \alpha^*), \quad (3.8)$$

and the squeezing operator,

$$\begin{aligned} \hat{a} \hat{S}(\xi) &= \hat{S}(\xi) [\hat{a} \cosh r - \hat{a}^\dagger e^{i\phi} \sinh r], \\ \hat{a}^\dagger \hat{S}(\xi) &= \hat{S}(\xi) [\hat{a}^\dagger \cosh r - \hat{a} e^{-i\phi} \sinh r]. \end{aligned} \quad (3.9)$$

Let us firstly compute  $N_{\text{Gauss}}$ , using the relations given by Eqs. 3.8 and 3.9 and the cyclic property of the trace. This is useful due to the unitarity of the displacement and squeezing operators. Then, the number of photons of a general Gaussian state (Eq. 3.6) is

$$\begin{aligned} N_{\text{Gauss}} &= \text{Tr}\left((\hat{a}^\dagger + \alpha^*)(\hat{a} + \alpha) \hat{S} \hat{\rho}_{\text{th}} \hat{S}^\dagger\right) \\ &= \text{Tr}\left((\hat{a}^\dagger \hat{a} + \alpha^* \hat{a} + \alpha \hat{a}^\dagger + |\alpha|^2) \hat{S} \hat{\rho}_{\text{th}} \hat{S}^\dagger\right) \\ &= \text{Tr}\left(\hat{a}^\dagger \hat{a} \hat{S} \hat{\rho}_{\text{th}} \hat{S}^\dagger\right) + \text{Tr}\left(|\alpha|^2 \hat{S} \hat{\rho}_{\text{th}} \hat{S}^\dagger\right) \\ &= |\alpha|^2 + \text{Tr}\left((\hat{a}^\dagger \cosh r - \hat{a} e^{-i\phi} \sinh r)(\hat{a} \cosh r - \hat{a}^\dagger e^{i\phi} \sinh r) \hat{\rho}_{\text{th}}\right) \\ &= |\alpha|^2 + \text{Tr}\left((\hat{n} \cosh^2 r + (\hat{n} + 1) \sinh^2 r) \hat{\rho}_{\text{th}}\right) \\ &= |\alpha|^2 + (2 \cosh^2 r - 1) n_{\text{th}} + \sinh^2 r, \end{aligned} \quad (3.10)$$

where  $\alpha$  defines the displacement,  $r$  the absolute value of the squeezing, and  $n_{\text{th}}$  the number of photons of the thermal state.

Notice that the denominator of Eq. 3.7 coincides with Eq. 3.10. The calculation of the numerator of  $N_{\text{PS}}$  gives

$$\begin{aligned}
\text{Num}_{\text{PS}} &= \text{Tr}\left((\hat{a}^\dagger + \alpha^*)(\hat{a}^\dagger + \alpha^*)(\hat{a} + \alpha)(\hat{a} + \alpha)\hat{S}\hat{\rho}_{\text{th}}\hat{S}^\dagger\right) \\
&= \text{Tr}\left((\hat{a}^{\dagger 2}\hat{a}^2 + \alpha^2\hat{a}^{\dagger 2} + \alpha^{*2}\hat{a}^2 + 4|\alpha|^2\hat{a}^\dagger\hat{a} + |\alpha|^4)\hat{S}\hat{\rho}_{\text{th}}\hat{S}^\dagger\right) \\
&= \text{Tr}\left(\left|\cosh^2 r\hat{a}^{\dagger 2} + \sinh^2 r\hat{a}^2 - e^{-i\phi}\sinh r\cosh r(2\hat{n} + 1)\right|^2\hat{\rho}_{\text{th}}\right) \\
&\quad - \text{Tr}\left((\alpha^2e^{-i\phi} + \alpha^{*2}e^{i\phi})\sinh r\cosh r(2\hat{n} + 1)\hat{\rho}_{\text{th}}\right) \\
&\quad + \text{Tr}\left(4|\alpha|^2(\cosh^2 r\hat{n} + \sinh^2 r(\hat{n} + 1))\hat{\rho}_{\text{th}}\right) + |\alpha|^4 \\
&= |\alpha|^4 - |\alpha|^2(2n_{\text{th}} + 1)\sinh(2r)\cos(2\theta - \phi) + 2(n_{\text{th}} + 1)^2\sinh^4(r) \\
&\quad + 2n_{\text{th}}^2\cosh^4(r) + 2|\alpha|^2((2n_{\text{th}} + 1)\cosh(2r) - 1) \\
&\quad + (8n_{\text{th}}(n_{\text{th}} + 1) + 1)\sinh^2(r)\cosh^2(r), \tag{3.11}
\end{aligned}$$

where  $\phi$  and  $\theta$  are respectively the squeezing and displacement phases.  $N_{\text{PS}}$ , obtained by replacing Eqs. 3.11 and 3.10 in Eq. 3.7, which results in

$$\begin{aligned}
N_{\text{PS}} &= \frac{|\alpha|^4 - |\alpha|^2((2n_{\text{th}} + 1)(\sinh(2r)\cos(\theta - 2\phi) - 2\cosh(2r)) + 2)}{|\alpha|^2 + 2n_{\text{th}}\cosh^2(r) - n_{\text{th}} + \sinh^2(r)} \\
&\quad + \frac{2n_{\text{th}}^2\cosh^4(r) + 2(n_{\text{th}} + 1)^2\sinh^4(r) + (8n_{\text{th}}^2 + 8n_{\text{th}} + 1)\sinh^2(r)\cosh^2(r)}{|\alpha|^2 + 2n_{\text{th}}\cosh^2(r) - n_{\text{th}} + \sinh^2(r)}. \tag{3.12}
\end{aligned}$$

In order to compare the number of photons before and after the operation, we calculate the difference of photons. Since the equation depends on five parameters, namely,  $|\alpha|$ ,  $r$ ,  $n_{\text{th}}$ ,  $\phi$ ,  $\theta$ , we focus on the relation between phases that give the smallest number of photons for the PS case, that is,  $2\theta = \phi$ . The difference between Eq. 3.12 and Eq. 3.10 ( $N_{\text{PS}} - N_{\text{Gaussian}}$ ) is

$$\Delta N = (2n_{\text{th}} + 1)\cosh(2r) - \frac{2(\alpha^2 + n_{\text{th}}^2 + n_{\text{th}}) + 2\alpha^2(2n_{\text{th}} + 1)\sinh(2r)}{2\alpha^2 + (2n_{\text{th}} + 1)\cosh(2r) - 1}, \tag{3.13}$$

which is depicted in Fig. 3.3. We have plotted the surface for small values of squeezing and displacement since we are interested in the regime of small photon number, which implies low values for  $r$  and  $\alpha$ .

By observing Fig. 3.3, we conclude that it is possible to decrease the number of photons of certain Gaussian states by photon subtraction. We are interested in the relation between squeezing and displacement which optimizes the photon number reduction. This relation is achieved by computing the gradient of Eq. 3.13. Specifically, the component corresponding to the derivative in  $r$  has been chosen, and the resulting equation is

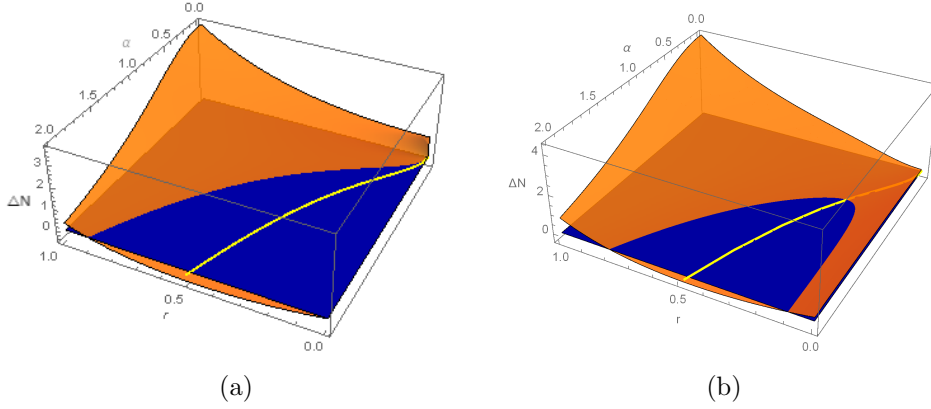


Figure 3.3: Representation of the difference in the number of photons ( $\Delta N$ ) given by Eq. 3.13, in terms of the absolute values of squeezing ( $r$ ) and displacement ( $\alpha$ ) of the Gaussian state for  $n_{\text{th}} = 0$  (a) and  $n_{\text{th}} = 0.1$  (b). The orange surface represents the difference of photons and the blue surface takes value 0, to serve as a reference. When the orange surface is greater than 0, the photon subtraction operation increases the number of photons but, when it is less than 0, the number of photons decreases. The yellow line (Eq. 3.14) represents the optimal combination of squeezing and displacement for a reduction in the photon number for a given  $n_{\text{th}}$ .

$$(2n_{\text{th}} + 1) (-8\alpha^2 + (2n_{\text{th}} + 1) \sinh(6r) + (8\alpha^2 - 4) \sinh(4r)) + (8(1 - 2\alpha^2) + 12n_{\text{th}}(n_{\text{th}} + 1) + 5) \sinh(2r) + 8(\alpha^2 - 2\alpha^4) \cosh(2r) = 0. \quad (3.14)$$

It can be expressed parametrically and it is represented graphically in Fig. 3.3, in which it is clear that the line actually corresponds to the minimum.

However, notice that, in the case of  $n_{\text{th}} > 0$  (Fig. 3.3b), there is a region for the optimal relation where photon subtraction increases the number of photons. Therefore, we must find another relation between the parameters to define the region for the optimal relation where the number of photons decrease. This is achieved by isolating one parameter in Eq. 3.14 and replacing it in Eq. 3.13. The obtained relation in the limit of high squeezing  $r$  is

$$r > \frac{1}{2} \ln \left( \frac{3}{2} (2n_{\text{th}} + 1) \right), \quad (3.15)$$

and, in the limit of low squeezing,

$$r > \frac{1}{2} \ln \left( \frac{2}{\sqrt{2} - 1} n_{\text{th}} + 1 \right). \quad (3.16)$$

The calculation of these inequalities is written down in the Appendix A.1 (Eq. A.1).



### 3.3 PS with Optimal Displacement and Squeezing

In Section 3.1, we have proven that photon subtraction does not provide any advantage when acting on a two-mode squeezed state, and that it doubles the number of photons for that state. Then, in Section 3.2, we have found a relation between squeezing and displacement for which photon subtraction actually reduces the number of photons of a single-mode Gaussian state. In this Section, we want to apply photon subtraction to a quantum state whose partial trace is the state found in the previous Section. There are infinite possible two-mode Gaussian states which fulfil this constraint, thus we will focus on the case which can be experimentally generated in a simplest manner. Indeed, we use a TMSS in order to entangle the signal and idler modes. Then, we apply the displacement  $\hat{D}(\alpha)$  and the squeezing  $\hat{S}(\xi)$  given by Eq. 3.14 and, finally, the photon subtraction operation,  $\hat{a}$ . This state is of the form

$$|SD\lambda\rangle = \frac{\hat{a}\hat{D}(\alpha)\hat{S}(\xi)|\lambda_{12}\rangle}{\langle\lambda_{12}|\hat{S}^\dagger(\xi)\hat{D}^\dagger(\alpha)\hat{a}^\dagger\hat{a}\hat{D}(\alpha)\hat{S}(\xi)|\lambda_{12}\rangle}, \quad (3.17)$$

where  $|\lambda_{12}\rangle$  is given by Eq. 2.9 and the normalization constant is  $\alpha^2 + N'(2\cosh^2(r) - 1) + \sinh^2(r)$ , where  $N'$  is the number of photons defined for the TMSS. Afterwards, we need to fix the number of photons sent to the object. In the previous Section, we also concluded that the optimal relation between the phases of displacement and squeezing is  $2\theta = \phi$ .

The calculation of the SNR follows the same steps as in the previous cases. Equations 3.8 and 3.9 are necessary, as well as the expectation values calculated in Sections 2.2 and 3.1. This time, the calculations will not be displayed here, but the needed expectation values will be written down in Appendix A.2. The expectation value of Eq. 2.10, depending on the parameters  $\alpha$ ,  $\xi$ ,  $\theta$  and  $\phi$ , results in

$$\langle\hat{b}_1\hat{b}_2 + \hat{b}_1^\dagger\hat{b}_2^\dagger\rangle_{SD\lambda} = \frac{2\sqrt{\eta N'(N'+1)}}{\alpha^2 - N' + 2N'\cosh^2(r) + \sinh^2(r)} \left( (6N' + 3)\cosh^3(r) - \alpha^2\sinh(r) + (2\alpha^2 - 4N' - 3)\cosh(r) \right) \quad (3.18)$$

where  $N'$  is the photon number for a TMSS. Notice that, after replacing  $2\theta = \phi$ , the result does not depend on the direction of squeezing  $\phi$ . This is because  $\phi$  and  $\theta$  depend on the choice of the coordinate system  $(x, p)$ , so the result can only depend on the relation between the phases. The expected

number of photons for the state given in Eq. 3.17 is

$$\begin{aligned}
\langle \hat{a}_1^\dagger \hat{a}_1 \rangle_{\text{SD}\lambda} &= \frac{2\alpha^2((2N' + 1) \cosh(2r) - 1) - \alpha^2(2N' + 1) \sinh(2r)}{\alpha^2 - N' + 2N' \cosh^2(r) + \sinh^2(r)} \\
&+ \frac{2(N' + 1)^2 \sinh^4(r) + (8N'^2 + 8N' + 1) \sinh^2(r) \cosh^2(r)}{\alpha^2 - N' + 2N' \cosh^2(r) + \sinh^2(r)} \\
&+ \frac{2N'^2 \cosh^4(r) + \alpha^4}{\alpha^2 - N' + 2N' \cosh^2(r) + \sinh^2(r)} = N
\end{aligned} \tag{3.19}$$

The equation obtained for  $\langle (\hat{b}_1 \hat{b}_2 + \hat{b}_1^\dagger \hat{b}_2^\dagger)^2 \rangle$  is

$$\begin{aligned}
\langle (\hat{b}_1 \hat{b}_2 + \hat{b}_1^\dagger \hat{b}_2^\dagger)^2 \rangle_{\text{SD}\lambda} &= \frac{8\alpha^4(2\eta N' + \eta) + 16\alpha^2(\eta(3N'^2 + N' - 1) + 1)}{4(2\alpha^2 + (2N' + 1) \cosh(2r) - 1)} \\
&+ \frac{8 \cosh(2r) (\eta(\alpha^2(22N'(N' + 1) + 2) + 2N'(N' + 1)(3N' - 4) - 1))}{4(2\alpha^2 + (2N' + 1) \cosh(2r) - 1)} \\
&- \frac{4 \cosh(2r)((\eta - 1)(8N'^2 + 6N' + 3) n_{\text{th}} - 2\eta((2N'(N' + 1) + 1)))}{4(2\alpha^2 + (2N' + 1) \cosh(2r) - 1)} \\
&+ \frac{\eta(N'(24N'^2 + 12N' - 2) + 5) - 12(2\alpha^2 - 1)(\eta - 1)n_{\text{th}}}{4(2\alpha^2 + (2N' + 1) \cosh(2r) - 1)} \\
&- \frac{8\alpha^2\eta(14N'(N' + 1) + 1) \sinh(2r)}{4(2\alpha^2 + (2N' + 1) \cosh(2r) - 1)} \\
&+ \frac{3\eta(2N' + 1)(20N'(N' + 1) + 1) \cosh(4r) - 8}{4(2\alpha^2 + (2N' + 1) \cosh(2r) - 1)}
\end{aligned} \tag{3.20}$$

By replacing Eqs. 3.18 and 3.20 in Eq. 2.1, we obtain the SNR for the signal (Eq. 3.17). Let us remember that we must compare the protocols using the same resources, so we have made a similar change in the number of photons performed for Eq. 3.4, but taking into account that now the number of photons of the signal is expressed by Eq. 3.19. This process is written down in Appendix A.2, along with the SNR (Eq. A.3).

It should be clarified that the parameter called  $N'$  in this Section, represents  $n_{\text{th}}$  in the previous one, since the thermal state of the Section 3.2 of single-mode photon subtraction is the resultant of tracing out the idler beam of a TMSS. In this Section,  $n_{\text{th}}$  comes from the interaction with the object.

The comparison will be done with the protocol exposed in Section 2.2, the quantum protocol with a Gaussian state with SNR given by Eq. 2.13. By computing the ratio between Eqs. A.3 (after replacing  $N'$  with Eq. A.6) and 2.13, we obtain the comparison between the Gaussian and the displaced squeezed photon subtracted TMSS, which is graphically represented in Fig. 3.4 for a single-mode squeezing value of  $r = 0.1$  and a reflectivity of  $\eta = 0.1$ .

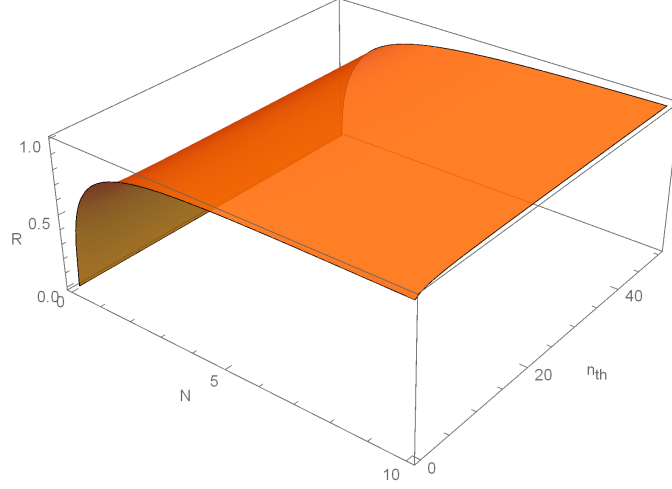


Figure 3.4: **Representation of the ratio ( $R$ ) between the SNRs of the quantum non-Gaussian protocol, with a signal expressed by Eq. 3.17, and the quantum Gaussian protocol with a signal state of the form of Eq. 2.9, in terms of the signal photons ( $N$ ) and thermal photons ( $n_{\text{th}}$ ). The values chosen for the reflectivity  $\eta$  and the single-mode squeezing  $r$  are  $\eta = r = 0.1$ .**

As it can be clearly seen, the surface stays below 1 for every signal and thermal photons in the studied range, which means that the non-Gaussian protocol developed in this Section is worse than the Gaussian one with a two-mode squeezed state. This result is fairly reasonable, since photons have been added to the state at the expense of the entanglement level in the process of squeezing and displacement. Indeed, the squeezing of the TMSS, represented by  $N'$ , has been reduced to compensate de number of photons. Additionally, this increment in the number of photons is not compensated by the photon subtraction operation.

In light of the results obtained in this Chapter, we can conclude that making the states non-Gaussian does not seem to provide any advantage in quantum illumination problems. Nevertheless, we have compared the best Gaussian protocol with a particular non-Gaussian protocol. This does not provide any general prove, since the employed state is only one of the infinite possible states that fit the conditions imposed in Section 3.2. Although a comparison with a general two-mode Gaussian state should be performed, we do not expect it to change the result for the aforementioned reasons.



# Conclusions

In this work, we have introduced the fundamentals of quantum illumination, with special emphasis on Gaussian states as a resource. We have shown that, indeed, the quantum Gaussian protocol outperforms the best classical one in the studied detection scheme. Photon subtraction is a common technique to de-Gaussianize quantum states in continuous variables. Motivated by an enhancement over the quantum Gaussian protocol using this technique reported in Ref. [2], we have studied it in detail, concluding that photon subtraction does not provide any advantage when the number of photons is fixed.

Below, the main results obtained throughout this work are described.

- We have compared the performance of the best quantum illumination protocol with Gaussian states against the best classical one by means of their respective signal-to-noise ratios. We have shown that the quantum protocol provides an enhancement in the limit of weak signal (small number of signal photons) with respect to the environmental noise photons. In this region of interest, the ratio reaches up to a maximum of 2.
- We have demonstrated that a protocol based on photon subtraction acting on a TMSS, does not overcome the aforementioned quantum protocol in the region of interest. The reason is that the growth of the number of photons of the signal that this operation generates must be compensated by reducing the squeezing level.
- We have studied the effect of photon subtraction in the photon number when applied to an arbitrary single-mode Gaussian state. We have found that, far from always increasing the number of photons, there exists a region of parameters ( $\alpha$ ,  $\xi$  and  $n_{\text{th}}$ ) for which the photon number is reduced. We have calculated the optimal relation between squeezing, displacement and thermal photons of a state for photon number reduction.
- We have used the aforesaid optimal relation to try to find a regime in which photon subtraction is advantageous. Indeed, we have applied

the annihilation operator to the signal mode of a TMSS, which we have previously displaced and squeezed an amount corresponding to the optimal relation among  $\alpha$ ,  $\xi$  and  $n_{\text{th}}$ . We have demonstrated that the new state still performs worse than the TMSS. This result can be understood based on the fact that the displacement and squeezing applied before the photon subtraction actually increase the photon number in comparison with the reduction caused by the photon subtraction. Therefore, for a given number of photons of the signal, the photons of the initial TMSS are reduced, which consequently decreases the entanglement.

The obtained results in this work concerning photon subtraction are a starting point for a more general study on its effects in quantum illumination protocols. In particular, a comparison between the TMSS and a general two-mode Gaussian state with photon subtraction should be carried out in order to definitely prove or deny the advantages given by this operation.

# Bibliography

- [1] Lorenzo Maccone and Changliang Ren. Quantum radar. *arXiv:1905.02672* (2019).
- [2] Longfei Fan and M. Suhail Zubairy. Quantum illumination using non-gaussian states generated by photon subtraction and photon addition. *Phys. Rev. A* **98**, 012319 (2018).
- [3] Seth Lloyd. Enhanced sensitivity of photodetection via quantum illumination. *Science* **321**, 1463-1465 (2008).
- [4] Zheshen Zhang, Maria Tengner, Tian Zhong, Franco N. C. Wong, and Jeffrey H. Shapiro. Entanglement's benefit survives an entanglement-breaking channel. *Phys. Rev. Lett.* **111**, 010501 (2013).
- [5] Christian Weedbrook, Stefano Pirandola, Raul Garcia-Patron, Nicolas J. Cerf, Timothy C. Ralph, Jeffrey H. Shapiro, and Seth Lloyd. Gaussian quantum information. *Rev. Mod. Phys.* **84**, 621 (2012).
- [6] William B. Case. Wigner functions and Weyl transforms for pedestrians. *American Journal of Physics* **76**, 937-946 (2008).
- [7] Jinglei Zhang. *Quantum Measurement and Preparation of Gaussian States*. PhD thesis, Aarhus University, Denmark (2018).
- [8] Alessandro Ferraro, Stefano Olivares, and Matteo G. A. Paris. Gaussian states in continuous variable quantum information. *Lecture Notes (Bibliopolis, Napoli)* (2005).
- [9] Thomas Durt and Vincent Debierre. Coherent states and the classical-quantum limit considered from the point of view of entanglement. *International Journal of Modern Physics B* **26**, 1245014 (2012).
- [10] Mikel Sanz, Urtzi Las Heras, Juan José García-Ripoll, Enrique Solano, and Roberto Di Candia. Quantum estimation methods for quantum illumination. *Phys. Rev. Lett.* **118**, 070803 (2017).

- [11] Mikel Sanz, Kirill G Fedorov, Frank Deppe, and Enrique Solano. Challenges in open-air microwave quantum communication and sensing. *2018 IEEE Conference on Antenna Measurements & Applications (CAMA)* (2018).
- [12] Alexei Ourjoumtsev, Rosa Tualle-Brouri, Julien Laurat, and Philippe Grangier. Generating optical Schrödinger kittens for quantum information processing. *Science* **312**, 83-86 (2006).



# Appendices



# Appendix A

## Intermediate Calculations

### A.1 Optimal Photon Reduction

In this Section, we present the photon number difference achieved by replacing  $\alpha$  in Eq. 3.13 using the expression given in Eq. 3.14. This operation results in

$$\Delta N_{opt} = \frac{m(y^4 + 2y^2 - 1) - 2y^3}{2y(y^2 - 1)} - \frac{\sqrt{m^2(y^8 - 2y^6 + 8y^4 - 2y^2 - 1) - 4my(y^4 + 2y^2 - 1) + 4y^4}}{2y(y^2 - 1)} \quad (\text{A.1})$$

where the parameters  $y$  and  $m$  are

$$y = \exp(2r), \quad m = 2n - 1.$$

The relation in Eq. 3.14 is valid when the expression given in Eq. A.1 is less than 0, i.e. when photon subtraction reduces the number of photons. Isolating the variable  $m$  we get

$$m < \frac{y^5 + 2y^3 + \sqrt{y^{10} - 2y^8 + 2y^6 - 2y^4 + y^2 - y}}{3y^4 - 1}. \quad (\text{A.2})$$

The high squeezing limit (Eq. 3.15) is obtained by taking the highest order component, and the low squeezing limit (Eq. 3.16) by generating a power series expansion around  $y = 1$  ( $r = 0$ ) to order 1.

### A.2 Optimal PS Protocol Expectation Values

In this Section, we write down the expectation values involved in the calculation of Eqs. 3.18 and 3.20, as well as the procedure we have followed to find the SNR of the optimal PS protocol.

First, the expectation values needed to compute the SNR are:

- $\langle \hat{a}_1 \hat{a}_2 \rangle_{\text{SD}\lambda} = \sqrt{N(N+1)} (\alpha^2 (2 \cosh(r) - \sinh(r) \cos(2\theta - \phi)))$   
 $+ \sqrt{N(N+1)} (\cosh(r) (-4N + 3(2N+1) \cosh^2(r) - 3))$
- $\langle \hat{a}_2^\dagger \hat{a}_2 \rangle_{\text{SD}\lambda} = \alpha^2 + N(2N+1) (2 \cosh^2(r) - 1) + \sinh^2(r)$
- $\langle \hat{a}_1^2 \hat{a}_2^2 \rangle_{\text{SD}\lambda} = 6\alpha^2 N(N+1) \cosh(r) (\cosh(r) - \sinh(r) \cos(2\theta - \phi))$   
 $+ 6N^2(N+1) \cosh^2(r) (2 \cosh^2(r) - 1) + 2N(N+1) \sinh^2(r) \cosh^2(r)$   
 $+ (2N(N+1) - 4N(3N+2)(N+1)) \sinh^2(r) \cosh^2(r)$
- $\langle \hat{a}_1^\dagger \hat{a}_1 \hat{a}_2^\dagger \hat{a}_2 \rangle_{\text{SD}\lambda} = \alpha^4 N - 2\alpha^2 (2(2N+1)N + N) \sinh(r) \cosh(r) \cos(2\theta - \phi)$   
 $+ 4\alpha^2 (N \sinh^2(r) + N(2N+1) (2 \cosh^2(r) - 1))$   
 $+ (8(3N+2)N^2 + 8(2N+1)N + N) \sinh^2(r) \cosh^2(r)$   
 $+ 2N^2(3N+2) \cosh^4(r) + 6N(N+1)^2 \sinh^4(r)$

Using the obtained expectation values, we find Eqs. 3.18 and 3.20. The SNR obtained via Eq. 2.1 is

$$\begin{aligned}
\text{SNR}_{\text{SD}\lambda} = & -4\eta \left( (8\alpha^2 + 2N' - 3) \cosh(r) - 4\alpha^2 \sinh(r) + (6N' + 3) \cosh(3r) \right)^2 \\
& N'(N'+1) [4(\eta - 1) (2\alpha^2 + (2N' + 1) \cosh(2r) - 1) ((2\alpha^2 - 1) (3n_{\text{th}} + 2) \\
& + (4N'(N'+1) + (8N'^2 + 6N' + 3) n_{\text{th}} + 2) \cosh(2r)) \\
& + 4\eta N'(N'+1) \left( (8\alpha^2 + 2N' - 3) \cosh(r) - 4\alpha^2 \sinh(r) \right. \\
& \left. + (6N' + 3) \cosh(3r) \right)^2 - \eta (2\alpha^2 + (2N' + 1) \cosh(2r) - 1) \\
& (8\alpha^4 + 12(4\alpha^2 + 1) N'^2 + 2(8(\alpha^4 + \alpha^2) - 1) N' + 24N'^3 \\
& + 16(\alpha^2(11N'(N'+1) + 1) + 3N'(N'^2 - 1)) \cosh(2r) \\
& - 8\alpha^2(14N'(N'+1) + 1) \sinh(2r) \\
& \left. + 3(2N' + 1)(20N'(N'+1) + 1) \cosh(4r) - 3 \right]^{-1}. \tag{A.3}
\end{aligned}$$

Now, we isolate  $\alpha$  in Eq. 3.14 and replace it in the number of photons of the signal (Eq. 3.19). This leads to the optimal number of photons of the signal, now dependent on two parameters,  $N'$  and  $r$ ,

$$\begin{aligned}
N = & e^{-2r} \frac{(2N' + 1)e^{12r} + (6N' + B + 3)e^{8r} - 10e^{6r} + (18N' - 5B + 9)e^{4r}}{8(e^{4r} - 1)} \\
& + e^{-2r} \frac{2e^{2r} - 5(2N' + 1)}{8(e^{4r} - 1)}, \tag{A.4}
\end{aligned}$$

$$\text{where} \tag{A.5}$$

$$\begin{aligned}
B = & [4(8N'(N'+1) + 3) + 2(2N'+1)^2 \sinh(8r) + 4(2N'+1) \sinh(2r) \\
& - 12(2N'+1) \cosh(2r) + 4(2N'+1) \cosh(6r) \\
& - 4(2N'+1) \sinh(6r) - 4(2N'+1)^2 \cosh(4r)]^{1/2}.
\end{aligned}$$

From this equation, we isolate  $N'$ , which results in two solutions. The positive solution, which is the physically valid one, is

$$\begin{aligned}
N' = & \frac{4[e^{16r}(2 \cosh(2r) - 3 \sinh(2r))^2 (8N^2 \sinh(8r) - 4(2N + 3)^2 \cosh(4r))}{2(e^{8r}(-4e^{4r} + 9e^{8r} + 84) - 25)} \\
& + \frac{4e^{16r}(16N + 17) \cosh(8r) + 32(N + 1)N + 19}{2(e^{8r}(-4e^{4r} + 9e^{8r} + 84) - 25)} \\
& + \frac{4(N + 1)e^{14r} - 10(2N + 3)e^{2r} + 2(6N + 13)e^{10r} + 4(9N + 16)e^{6r}}{2(e^{8r}(-4e^{4r} + 9e^{8r} + 84) - 25)} \\
& + \frac{4e^{12r} - 84e^{8r} - 9e^{16r} + 25}{2(e^{8r}(-4e^{4r} + 9e^{8r} + 84) - 25)}. \tag{A.6}
\end{aligned}$$

We replace it in the SNR (Eq. A.3), so the SNR now depends on the photons of the signal  $N$ , and not  $N'$ . The comparison with the Gaussian protocol is depicted in Fig. 3.4.



## Appendix B

# Mathematica Programs

### B.1 Representation in Phase Space of different Wigner Functions

In this program, we plot the Wigner functions for different Gaussian states (Eqs. 1.17, 1.18 and 1.19). The graphics are the ones depicted in Fig. 1.1.

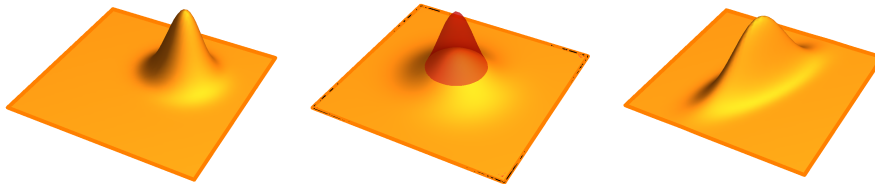
```

Thermal[x_, p_, λ_] := (1 - λ) / (π ħ (1 + λ)) Exp[-1 / ħ ((1 - λ) / (1 + λ)) (x^2 + p^2)]
Coherent[x_, p_, α_] :=
  (1 / (π ħ)) Exp[-1 / ħ ((x - Re[α] / (Sqrt[2 ħ]))^2 + (p - Im[α] / (Sqrt[2 ħ]))^2)]
Squeezed[x_, p_, α_, r_, θ_] :=
  (1 / (π ħ)) Exp[-Abs[Cosh[r] Exp[-i θ] ((x - Re[α] + i (p - Im[α])) / (Sqrt[2 ħ])) +
    Sinh[r] Exp[i θ] ((x - Re[α] - i (p - Im[α])) / (Sqrt[2 ħ]))]^2]

ħ = 1;

plot1 = Plot3D[Coherent[x, p, 1.5 (1 + i)], {x, -4, 4}, {p, -4, 4},
  PlotRange → All, PlotPoints → 70, Mesh -> None, AxesLabel → {"x", "p"},
  Boxed → False, Axes → False, BoundaryStyle → Directive[Orange, Thick]]
plot2 := Plot3D[Thermal[x, p, 0.4], {x, -4, 4}, {p, -4, 4}, PlotRange → All,
  PlotPoints → 50, Mesh -> None, AxesLabel → {"x", "p"}, Boxed → False,
  Axes → False, BoundaryStyle → Directive[Orange, Thick]]
plot3 := Plot3D[Thermal[x, p, 0], {x, -4, 4}, {p, -4, 4}, PlotRange → All,
  PlotPoints → 50, Mesh -> None, AxesLabel → {"x", "p"}, Boxed → False,
  Axes → False, PlotStyle → Directive[Red, Opacity[0.5]]]
Show[plot2, plot3]
plot4 = Plot3D[Squeezed[x, p, 0, 0.5, -π / 8], {x, -5, 5}, {p, -5, 5},
  PlotRange → All, PlotPoints → 70, Mesh -> None, AxesLabel → {"x", "p"},
  Boxed → False, Axes → False, BoundaryStyle → Directive[Orange, Thick]]

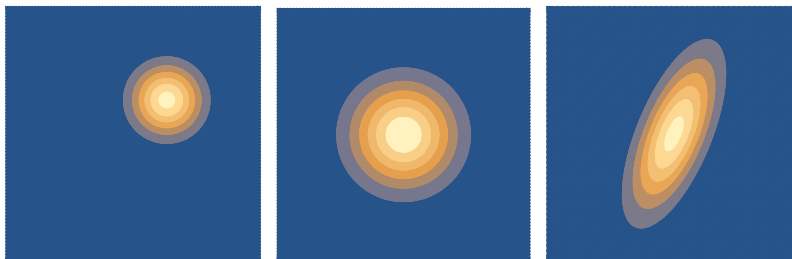
```



```

cplot1 = ContourPlot[Coherent[x, p, 1.5 (1 + i)], {x, -4, 4}, {p, -4, 4},
  PlotRange → All, PlotPoints → 80, ContourStyle → None, Frame → False]
cplot2 = ContourPlot[Thermal[x, p, 0.4], {x, -4, 4}, {p, -4, 4},
  PlotRange → All, PlotPoints → 80, ContourStyle → None, Frame → False]
cplot3 = ContourPlot[Squeezed[x, p, 0, 0.5, -π / 8], {x, -4, 4}, {p, -4, 4},
  PlotRange → All, PlotPoints → 50, ContourStyle → None, Frame → False]

```





## **B.2 Representation of SNR Comparisons**

In this program, we represent the ratio between the SNR of different protocols. First, we compare the classical protocol with the quantum Gaussian protocol (Fig. 2.3). Then, the Gaussian protocol with the PS protocol (Fig. 3.1) and, finally, both quantum protocols with the classical one (Fig. 3.2).

```
In[1]:= xcua =  $\eta (N + 1) (6 N + 1) + (1 - \eta) (2 N t + N + t + 1)$ ;
x = 2 Sqrt[ $\eta N (N + 1)$ ];
```

```
In[15]:= SNRQ1 = (x^2) / (xcua - x^2) // FullSimplify
```

```
Out[15]= 
$$\frac{4 \eta N (1 + N)}{1 + N + 2 \eta N (1 + N) - t (-1 + \eta) (1 + 2 N)}$$

```

```
In[20]:= SNRC[ $\eta$ _, N_, t_] := (2 N  $\eta$ ) / ((1 -  $\eta$ ) t + 1 / 2)
```

```
SNRQ[ $\eta$ _, N_, t_] := 
$$\frac{4 \eta N (1 + N)}{1 + N + 2 \eta N (1 + N) - t (-1 + \eta) (1 + 2 N)}$$

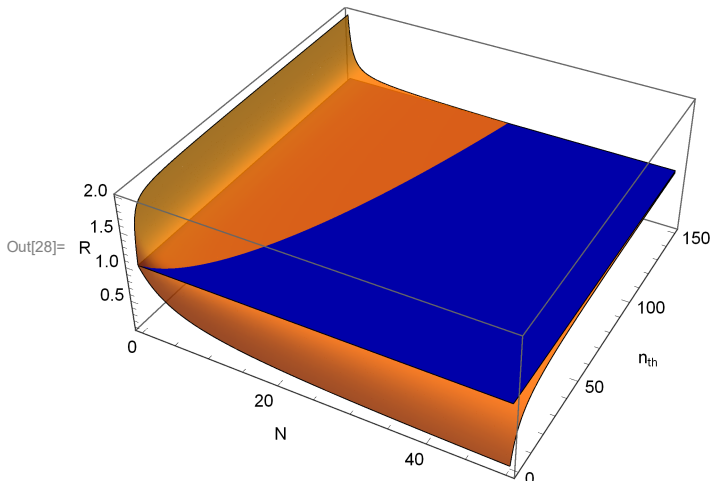
```

```
ComparisonQC[ $\eta$ _, N_, t_] := SNRQ[ $\eta$ , N, t] / SNRC[ $\eta$ , N, t]
```

```
In[53]:= Plot1 :=
```

```
Plot3D[1, {n, 0, 50}, {t, 0, 150}, PlotPoints -> 150, PlotRange -> All, Mesh -> None,
AxesLabel -> {"N", Subscript["n", "th"], "R"}, PlotStyle -> Directive[Blue]]
PlotQC := Plot3D[ComparisonQC[0.1, n, t], {n, 0, 50}, {t, 0, 150}, PlotPoints -> 150,
PlotRange -> All, Mesh -> None, AxesLabel -> {"N", Subscript["n", "th"], "R"},
PlotStyle -> Directive[Orange, Opacity[0.85]]]
```

```
In[28]:= Show[Plot1, PlotQC]
```



Now with photon subtraction:

```
In[29]:= ps = 4 Sqrt[ $\eta N (N + 1)$ ];
```

```
pscua = 2  $\eta$  (12 N^2 + 12 N + 1) + (1 -  $\eta$ ) (t (4 N + 3) + 2 N + 2);
```

```
SNRQP = ps^2 / (pscua - ps^2) // FullSimplify
```

```
Out[31]= 
$$\frac{16 \eta N (1 + N)}{2 (1 + N) + (3 + 4 N) (t - t \eta + 2 \eta N)}$$

```

```
In[39]:= SNRQPS[ $\eta$ _, N_, t_] := 
$$\frac{16 \eta N (1 + N)}{2 (1 + N) + (3 + 4 N) (t - t \eta + 2 \eta N)}$$

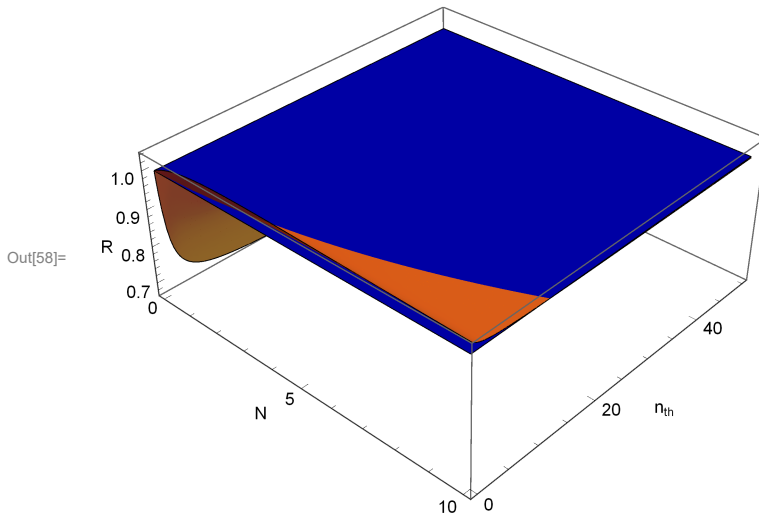
```

```
ComparisonPSQ[ $\eta$ _, N_, t_] := SNRQPS[ $\eta$ , N / 2, t] / SNRQ[ $\eta$ , N, t]
```

```
In[55]:= Plot2 :=
```

```
Plot3D[1, {n, 0, 10}, {t, 0, 50}, PlotPoints -> 150, PlotRange -> All, Mesh -> None,
AxesLabel -> {"N", Subscript["n", "th"], "R"}, PlotStyle -> Directive[Blue]]
PlotPSQ := Plot3D[ComparisonPSQ[0.1, n, t], {n, 0, 10},
{t, 0, 50}, PlotPoints -> 150, PlotRange -> All, Mesh -> None,
AxesLabel -> {"N", Subscript["n", "th"], "R"},
PlotStyle -> Directive[Orange, Opacity[0.85]]]
```

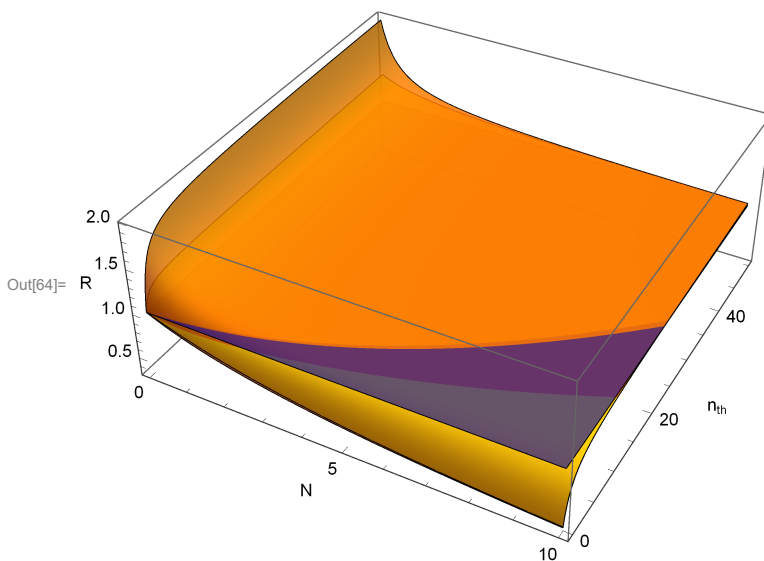
In[58]:= Show[Plot2, PlotPSQ]



In[48]:= ComparisonPSC[ $\eta$ \_, N\_, t\_] := SNRQPS[ $\eta$ , N/2, t] / SNRC[ $\eta$ , N, t]

In[59]:= PlotPSQ := Plot3D[ComparisonPSQ[0.1, n, t],  
 {n, 0, 10}, {t, 0, 50}, PlotPoints → 150, PlotRange → All,  
 Mesh → None, AxesLabel → {"N", Subscript["n", "th"], "R"},  
 PlotStyle → Directive[Orange, Opacity[0.85]]]  
 PlotPSC := Plot3D[ComparisonPSC[0.1, n, t], {n, 0, 10},  
 {t, 0, 50}, PlotPoints → 150, PlotRange → All, Mesh → None,  
 AxesLabel → {"N", Subscript["n", "th"], "R"},  
 PlotStyle → Directive[Yellow, Opacity[0.85]]]  
 Plot2QC := Plot3D[ComparisonQC[0.1, n, t], {n, 0, 10}, {t, 0, 50}, PlotPoints → 150,  
 PlotRange → All, Mesh → None, AxesLabel → {"N", Subscript["n", "th"], "R"},  
 PlotStyle → Directive[Orange, Opacity[0.85]]]  
 Plot3 := Plot3D[1, {n, 0, 10}, {t, 0, 50}, PlotPoints → 150, PlotRange → All,  
 Mesh → None, AxesLabel → {"N", Subscript["n", "th"], "R"},  
 PlotStyle → Directive[Blue, Opacity[0.6]]]

In[64]:= Show[Plot2QC, PlotPSC, Plot3]



### **B.3 Optimal Displacement and Squeezing Calculation and Graphic Representation**

In this program, we represent the difference of photons generated by photon subtraction (Eq. 3.13) and find the optimal relation between the parameters  $r$ ,  $\alpha$  and  $n_{\text{th}}$ . We choose  $n_{\text{th}} = 0$  and  $n_{\text{th}} = 0.1$  just for graphic representation (Fig. 3.3).

```

num = Cosh[r]^4 + 2 * n^2 + Sinh[r]^4 * (2 n^2 + 4 n + 2) +
      Sinh[r]^2 Cosh[r]^2 (8 n^2 + 8 n + 1) - 2 alpha^2 Sinh[r] Cosh[r] (2 n + 1) Cos[theta - 2 phi] +
      4 alpha^2 ((2 Cosh[r]^2 - 1) n + Sinh[r]^2) + alpha^4;
np = alpha^2 + (2 Cosh[r]^2 - 1) n + Sinh[r]^2;
npp = num / np;
dif = FullSimplify[npp - np];

```

```
dif
```

```

(1 - 4 alpha^2 + 2 (1 + 2 n) (-1 + 2 alpha^2) Cosh[2 r] + (1 + 2 n)^2 Cosh[4 r] - 4 (1 + 2 n) alpha^2 Sinh[2 r]) /
(2 (-1 + 2 alpha^2 + (1 + 2 n) Cosh[2 r])) // FullSimplify

```

```

(1 + 2 n) Cosh[2 r] + (-2 (n + n^2 + alpha^2) - 2 (1 + 2 n) alpha^2 Sinh[2 r]) /
(-1 + 2 alpha^2 + (1 + 2 n) Cosh[2 r])

```

```

ReplaceAll[(1 - 4 alpha^2 + 2 (1 + 2 n) (-1 + 2 alpha^2) Cosh[2 r] + (1 + 2 n)^2 Cosh[4 r] -
4 (1 + 2 n) alpha^2 Cos[theta - 2 phi] Sinh[2 r]) / (2 (-1 + 2 alpha^2 + (1 + 2 n) Cosh[2 r]))], {theta -> 2 phi}]

```

```

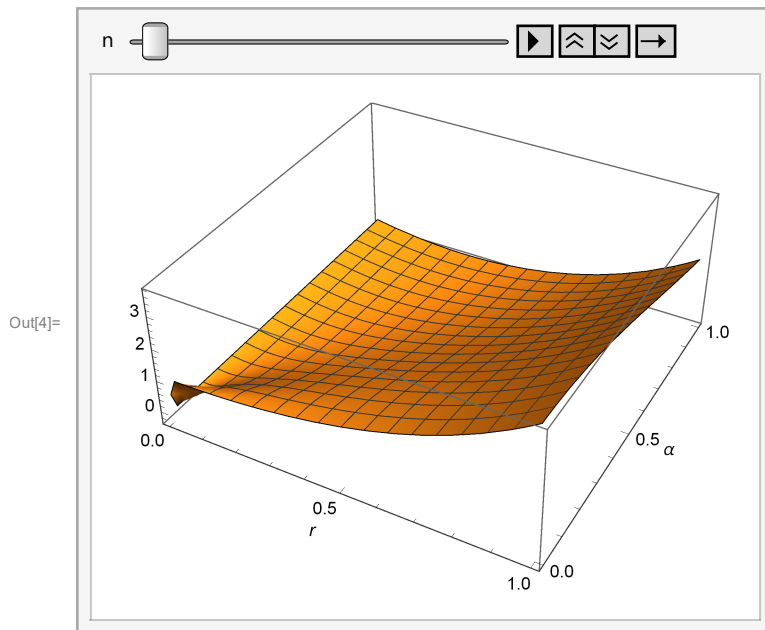
(1 - 4 alpha^2 + 2 (1 + 2 n) (-1 + 2 alpha^2) Cosh[2 r] + (1 + 2 n)^2 Cosh[4 r] - 4 (1 + 2 n) alpha^2 Sinh[2 r]) /
(2 (-1 + 2 alpha^2 + (1 + 2 n) Cosh[2 r]))

```

```

In[4]:= Animate[Plot3D[(1 - 4 alpha^2 + 2 (1 + 2 n) (-1 + 2 alpha^2) Cosh[2 r] + (1 + 2 n)^2 Cosh[4 r] -
4 (1 + 2 n) alpha^2 Sinh[2 r]) / (-2 + 4 alpha^2 + (2 + 4 n) Cosh[2 r]), {r, 0, 1},
{alpha, 0, 1}, AxesLabel -> Automatic], {n, 0, 1}, AnimationRunning -> False]

```



Since there exists a minimum, we compute the gradient of the function. In particular, the derivative in  $r$ :

```
FullSimplify[
  Derivative[1][
    ((1 - 4 \alpha^2 + 2 (1 + 2 n) (-1 + 2 \alpha^2) Cosh[2 r] + (1 + 2 n)^2 Cosh[4 r] - 4 (1 + 2 n)
      \alpha^2 Sinh[2 r]) / (-2 + 4 \alpha^2 + (2 + 4 n) Cosh[2 r]))]
  2 (1 + 2 n)
  (
    - (2 \alpha^2 (1 + 2 n + (-1 + 2 \alpha^2) Cosh[2 r]) /
      (-1 + 2 \alpha^2 + (1 + 2 n) Cosh[2 r])^2) +
    (1 + (2 (n + n^2 + \alpha^2) /
      (-1 + 2 \alpha^2 + (1 + 2 n) Cosh[2 r])^2)) Sinh[2 r]
  )
]
```

Numerator:

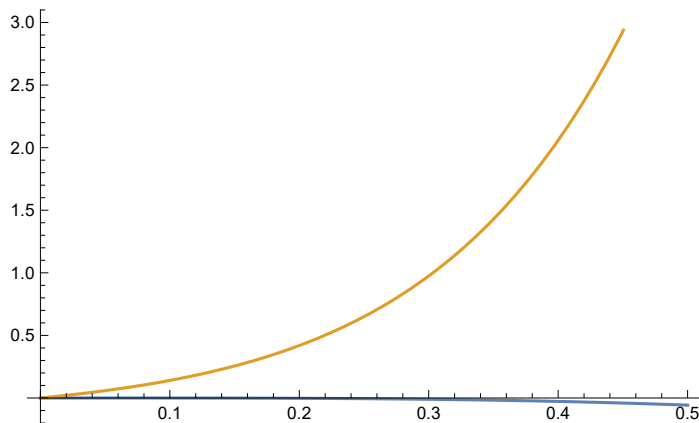
```
(-8 \alpha^2 Cos[\theta - 2 \phi] (1 + 2 n + (-1 + 2 \alpha^2) Cosh[2 r]) + (5 + 12 n (1 + n) - 8 \alpha^2 + 16 \alpha^4)
  Sinh[2 r] + (1 + 2 n) ((-4 + 8 \alpha^2) Sinh[4 r] + (1 + 2 n) Sinh[6 r])) /. {n -> 0, \theta -> 2 \phi}
-8 \alpha^2 (1 + (-1 + 2 \alpha^2) Cosh[2 r]) +
(5 - 8 \alpha^2 + 16 \alpha^4) Sinh[2 r] + (-4 + 8 \alpha^2) Sinh[4 r] + Sinh[6 r]
```

The numerator must be 0, so we can solve for  $\alpha^2$

```
Solve[ReplaceAll[-8 \alpha^2 (1 + (-1 + 2 \alpha^2) Cosh[2 r]) + (5 - 8 \alpha^2 + 16 \alpha^4) Sinh[2 r] +
  (-4 + 8 \alpha^2) Sinh[4 r] + Sinh[6 r], {\alpha^2 -> x, \alpha^4 -> x^2}] == 0, x]
{{x ->
  (-1 + Cosh[2 r] - Sinh[2 r] + Sinh[4 r] - \sqrt{2} \sqrt{(-2 Sinh[r]^2 + 2 Cosh[2 r] Sinh[r]^2 + 2
    Cosh[4 r] Sinh[r]^2 - Sinh[r]^2 Sinh[2 r] + Sinh[r]^2 Sinh[6 r])}) /
  (4 (Cosh[2 r] - Sinh[2 r]))}, {x -> (-1 + Cosh[2 r] - Sinh[2 r] + Sinh[4 r] +
  \sqrt{2} \sqrt{(-2 Sinh[r]^2 + 2 Cosh[2 r] Sinh[r]^2 + 2 Cosh[4 r] Sinh[r]^2 -
    Sinh[r]^2 Sinh[2 r] + Sinh[r]^2 Sinh[6 r])}) / (4 (Cosh[2 r] - Sinh[2 r]))}}
```

We plot both results for  $\alpha^2$  to see which of them is the correct one

```
Plot[
  {
    (-1 + Cosh[2 r] - Sinh[2 r] + Sinh[4 r] - \sqrt{2} \sqrt{(-2 Sinh[r]^2 + 2 Cosh[2 r] Sinh[r]^2 +
      2 Cosh[4 r] Sinh[r]^2 - Sinh[r]^2 Sinh[2 r] + Sinh[r]^2 Sinh[6 r])}) /
    (4 (Cosh[2 r] - Sinh[2 r])),
    (-1 + Cosh[2 r] - Sinh[2 r] + Sinh[4 r] + \sqrt{2}
      \sqrt{(-2 Sinh[r]^2 + 2 Cosh[2 r] Sinh[r]^2 + 2 Cosh[4 r] Sinh[r]^2 - Sinh[r]^2 Sinh[2 r] +
        Sinh[r]^2 Sinh[6 r])}) / (4 (Cosh[2 r] - Sinh[2 r]))
  }, {r, 0, 0.5}]
```



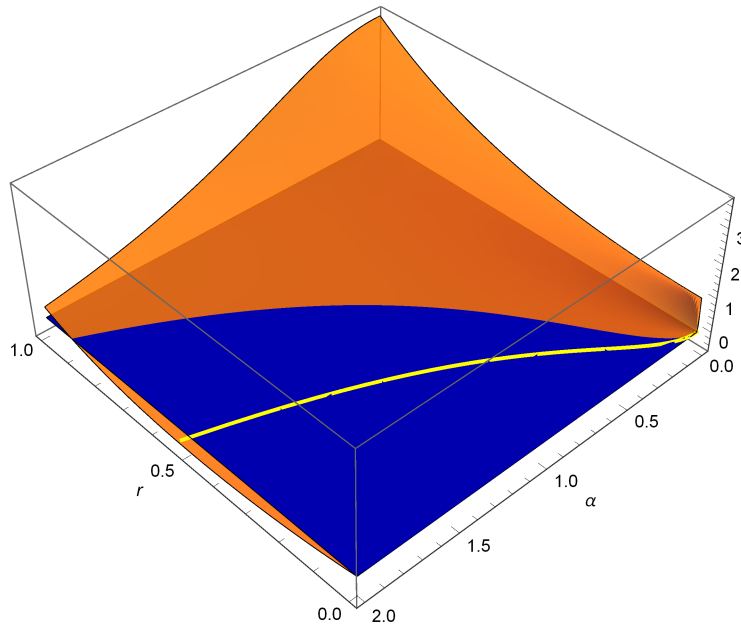
Notice that the first solution (blue) is negative, which is not possible for  $\alpha^2$ . We plot the line paramet-

rically along with the surface, to see if it is the minimum or not:

```

line := ParametricPlot3D[{r, Sqrt[
  (-1 + Cosh[2 r] - Sinh[2 r] + Sinh[4 r] + Sqrt[2] Sqrt[-2 Sinh[r]^2 + 2 Cosh[2 r] Sinh[r]^2 +
    2 Cosh[4 r] Sinh[r]^2 - Sinh[r]^2 Sinh[2 r] + Sinh[r]^2 Sinh[6 r]])] /
  (4 (Cosh[2 r] - Sinh[2 r]))], 0}, {r, 0, 1}, PlotStyle -> {Thick, Yellow}]
surface := Plot3D[Cosh[2 r] - (2 alpha^2 (1 + Sinh[2 r])) / (-1 + 2 alpha^2 + Cosh[2 r]), {r, 0, 1}, {alpha, 0, 2},
  AxesLabel -> Automatic, PlotPoints -> 100, PlotRange -> Automatic,
  Mesh -> None, PlotStyle -> Directive[Orange, Opacity[0.85]]]
zero := Plot3D[0, {r, 0, 1}, {alpha, 0, 2}, AxesLabel -> Automatic, PlotPoints -> 100,
  PlotRange -> Automatic, Mesh -> None, PlotStyle -> Directive[Blue]]
Show[surface, zero, line]

```



```

Solve[ReplaceAll[
  (-8 alpha^2 (1 + 2 n + (-1 + 2 alpha^2) Cosh[2 r]) + (5 + 12 n (1 + n) - 8 alpha^2 + 16 alpha^4) Sinh[2 r] +
  (1 + 2 n) ((-4 + 8 alpha^2) Sinh[4 r] + (1 + 2 n) Sinh[6 r])),
  {n -> 0.1, alpha^2 -> x, alpha^4 -> x^2}] == 0, x]

```

Solve::ratnz: Solve was unable to solve the system with inexact coefficients. The

answer was obtained by solving a corresponding exact system and numericizing the result. >>

```

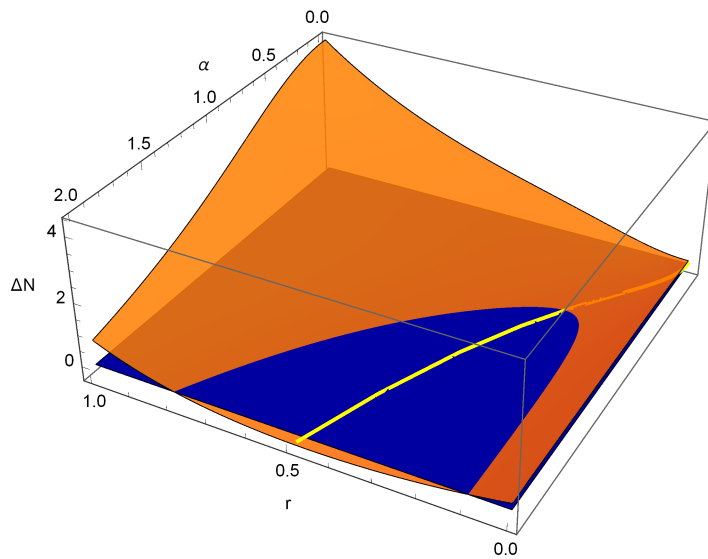
{{x -> (0.05 (-6. + 5. Cosh[2. r] - 5. Sinh[2. r] + 6. Sinh[4. r] -
  1. Sqrt[97. - 90. Cosh[2. r] - 36. Cosh[4. r] + 30. Cosh[6. r] + 30. Sinh[2. r] -
  30. Sinh[6. r] + 18. Sinh[8. r])) / (Cosh[2. r] - 1. Sinh[2. r])},
{x -> (0.05 (-6. + 5. Cosh[2. r] - 5. Sinh[2. r] + 6. Sinh[4. r] +
  Sqrt[97. - 90. Cosh[2. r] - 36. Cosh[4. r] + 30. Cosh[6. r] + 30. Sinh[2. r] -
  30. Sinh[6. r] + 18. Sinh[8. r])) / (Cosh[2. r] - 1. Sinh[2. r])}}

```

```

Surf :=
Plot3D[{ReplaceAll[(1 - 4 α2 + 2 (1 + 2 n) (-1 + 2 α2) Cosh[2 r] + (1 + 2 n)2 Cosh[4 r] -
4 (1 + 2 n) α2 Sinh[2 r]) / (-2 + 4 α2 + (2 + 4 n) Cosh[2 r]), n → 0.1]},
{r, 0, 1}, {α, 0, 2}, AxesLabel → {"r", "α", "ΔN"}, PlotPoints → 100,
PlotRange → Automatic, Mesh → None,
PlotStyle → Directive[Orange, Opacity[0.85]]]
li := ParametricPlot3D[
{r, Sqrt[(0.05` (-6.` + 5.` Cosh[2.` r] - 5.` Sinh[2.` r] + 6.` Sinh[4.` r] +
√(97.` - 90.` Cosh[2.` r] - 36.` Cosh[4.` r] + 30.` Cosh[6.` r] +
30.` Sinh[2.` r] - 30.` Sinh[6.` r] + 18.` Sinh[8.` r])) /
(Cosh[2.` r] - 1.` Sinh[2.` r])], 0}, {r, 0, 4}, PlotStyle → {Thick, Yellow}]
Show[Surf, li, zero]

```





## **B.4 Comparison between the Gaussian and Squeezed Displaced PS Protocols**

In this program, we find the SNR of the squeezed displaced PS protocol (Eq. A.3), and then we compare it with the Gaussian protocol (Eq. 2.7).

These are the needed expectation values for the calculation of the SNR

```
In[8]:= norm[N_, α_, r_] := Sinh[r]^2 + (2 Cosh[r]^2 - 1) N + α^2
n1[N_, α_, r_, θ_, φ_] := 2 Cosh[r]^4 N^2 +
  2 Sinh[r]^4 (N+1)^2 + Sinh[r]^2 Cosh[r]^2 (4 N (2 N+1) + 4 N+1) + α^4 +
  4 α^2 ((2 Cosh[r]^2 - 1) N + Sinh[r]^2) - 2 α^2 Cos[2 θ - φ] Sinh[r] Cosh[r] (2 N+1)
n2[N_, α_, r_] := Sinh[r]^2 + (2 Cosh[r]^2 - 1) N (2 N+1) + α^2
ala2[N_, α_, r_, θ_, φ_] := Sqrt[N (N+1)]
  (Cosh[r] (3 Cosh[r]^2 (2 N+1) - 4 N - 3) + α^2 (2 Cosh[r] - Sinh[r] Cos[2 θ - φ]))
nln2[N_, α_, r_, θ_, φ_] := Cosh[r]^4 (2 N^2 (3 N+2)) + Sinh[r]^4 (6 N (N+1)^2) +
  Sinh[r]^2 Cosh[r]^2 (8 N^2 (3 N+2) + 8 N (2 N+1) + N) +
  N α^4 + 4 α^2 ((2 Cosh[r]^2 - 1) N (2 N+1) + N Sinh[r]^2) -
  2 α^2 Cos[2 θ - φ] Sinh[r] Cosh[r] (2 N (2 N+1) + N)
alala2a2[N_, α_, r_, θ_, φ_] :=
  6 α^2 N (N+1) Cosh[r] (Cosh[r] - Sinh[r] Cos[2 θ - φ]) +
  Cosh[r]^2 (2 Cosh[r]^2 - 1) 6 N^2 (N+1) + Sinh[r]^2 Cosh[r]^2 2 N (N+1) +
  Cosh[r]^2 Sinh[r]^2 (2 (2 N (3 N+2) (N+1)) + 2 N (N+1))
```

```
In[14]:= Operator[η_, N_, α_, r_] := Sqrt[η] (2 ala2[N, α, r, 0, 0] / norm[N, α, r])
Operator2[η_, N_, nth_, α_, r_] :=
  η (2 alala2a2[N, α, r, 0, 0] / norm[N, α, r] + 2 nln2[N, α, r, 0, 0] / norm[N, α, r] +
    n1[N, α, r, 0, 0] / norm[N, α, r] + n2[N, α, r] / norm[N, α, r] + 1) +
  (1 - η) (2 nth n2[N, α, r] / norm[N, α, r] + nth + n2[N, α, r] / norm[N, α, r] + 1)
```

The following relation gives the OPTIMAL displacement in terms of the thermal photons of a single-mode gaussian state and the squeezing.

```
In[20]:= Alfa[nth_, r_] :=
  Sqrt[(-2 - 4 nth + 2 Cosh[2 r] - 2 Sinh[2 r] + 2 Sinh[4 r] + 4 nth Sinh[4 r] +
    Sqrt[6 + 16 nth + 16 nth^2 - 6 Cosh[2 r] - 12 nth Cosh[2 r] - 2 Cosh[4 r] -
      8 nth Cosh[4 r] - 8 nth^2 Cosh[4 r] + 2 Cosh[6 r] + 4 nth Cosh[6 r] +
      2 Sinh[2 r] + 4 nth Sinh[2 r] - 2 Sinh[6 r] - 4 nth Sinh[6 r] + Sinh[8 r] +
      4 nth Sinh[8 r] + 4 nth^2 Sinh[8 r]]) / (8 (Cosh[2 r] - Sinh[2 r]))]
```

```
In[21]:= Op[η_, N_, nth_, r_] := Operator[η, N, Alfa[N, r], r]^2
Op2[η_, N_, nth_, r_] := Operator2[η, N, nth, Alfa[N, r], r]
```

```
In[23]:= SNR[η_, N_, nth_, r_] := Op[η, N, nth, r] / (Op2[η, N, nth, r] - Op[η, N, nth, r])
```

The SNR depends, among other things, depends on the photon number of the TMSS. We want it to depend on the photon number of the signal.

The number of photons of the signal is:

```
NFot[N_, α_, r_] := n1[N, α, r, 0, 0] / norm[N, α, r]
```

The number of photons of the TMSS in terms of the ones of the signal:

**Solve[NFot[N, Alfa[N, r], r] == n, N]**

$$\text{Out[118]= } \left\{ \left\{ N \rightarrow \left( 25 - 30 e^{2r} + 64 e^{6r} - 84 e^{8r} + 26 e^{10r} + 4 e^{12r} + 4 e^{14r} - 9 e^{16r} - 20 e^{2r} n + 36 e^{6r} n + 12 e^{10r} n + 4 e^{14r} n - \sqrt{2} \sqrt{\left( 425 e^{4r} - 1070 e^{8r} + 1327 e^{12r} - 1316 e^{16r} + 823 e^{20r} - 206 e^{24r} + 17 e^{28r} + 400 e^{4r} n - 1360 e^{8r} n + 2096 e^{12r} n - 1888 e^{16r} n + 944 e^{20r} n - 208 e^{24r} n + 16 e^{28r} n - 200 e^{4r} n^2 - 320 e^{8r} n^2 + 1752 e^{12r} n^2 - 1056 e^{16r} n^2 + 424 e^{20r} n^2 - 96 e^{24r} n^2 + 8 e^{28r} n^2 \right)} \right) / \left( 2 \left( -25 + 84 e^{8r} - 4 e^{12r} + 9 e^{16r} \right) \right) \right\}, \left\{ N \rightarrow \left( 25 - 30 e^{2r} + 64 e^{6r} - 84 e^{8r} + 26 e^{10r} + 4 e^{12r} + 4 e^{14r} - 9 e^{16r} - 20 e^{2r} n + 36 e^{6r} n + 12 e^{10r} n + 4 e^{14r} n + \sqrt{2} \sqrt{\left( 425 e^{4r} - 1070 e^{8r} + 1327 e^{12r} - 1316 e^{16r} + 823 e^{20r} - 206 e^{24r} + 17 e^{28r} + 400 e^{4r} n - 1360 e^{8r} n + 2096 e^{12r} n - 1888 e^{16r} n + 944 e^{20r} n - 208 e^{24r} n + 16 e^{28r} n - 200 e^{4r} n^2 - 320 e^{8r} n^2 + 1752 e^{12r} n^2 - 1056 e^{16r} n^2 + 424 e^{20r} n^2 - 96 e^{24r} n^2 + 8 e^{28r} n^2 \right)} \right) / \left( 2 \left( -25 + 84 e^{8r} - 4 e^{12r} + 9 e^{16r} \right) \right) \right\} \right\}$$

$$\text{In[122]= } \text{NTMSS}[n_, r_] := \left( 25 - 84 e^{8r} + 4 e^{12r} - 9 e^{16r} + 4 e^{14r} (1+n) - 10 e^{2r} (3+2n) + 2 e^{10r} (13+6n) + 4 e^{6r} (16+9n) + 4 \sqrt{\left( e^{16r} (2 \text{Cosh}[2r] - 3 \text{Sinh}[2r])^2 (19+32n(1+n) - 4(3+2n)^2 \text{Cosh}[4r] + (17+16n) \text{Cosh}[8r] + 8n^2 \text{Sinh}[8r]) \right)} \right) / \left( 2 \left( -25 + e^{8r} (84 - 4 e^{4r} + 9 e^{8r}) \right) \right)$$

$$\text{In[123]= } \text{SNRQ1}[\eta_, N_, t_] := \frac{4 \eta N (1+N)}{1+N+2 \eta N (1+N) - t (-1+\eta) (1+2N)}$$

$$\text{SNRC}[\eta_, N_, t_] := (2 N \eta) / ((1-\eta) t + 1/2)$$

$$\text{In[81]= } \text{CompFin}[\eta_, N_, t_, r_] := \text{SNR}[\eta, \text{NTMSS}[N, r], t, r] / \text{SNRQ1}[\eta, N, t]$$

**In[109]=** **Comp** := **Plot3D**[{**CompFin**[0.1, n, t, 0.1]}, {n, **NFot**[0, **Alfa**[0, 0.1], 0.1], 10}, {t, 0, 50}, **PlotPoints** → 50, **PlotRange** → **All**, **Mesh** → **None**, **AxesLabel** → {"N", **Subscript**["n", "th"], "R"}, **PlotStyle** → **Directive**[**Orange**, **Opacity**[0.85]]] **Zero** := **Plot3D**[1, {n, 0, 10}, {t, 0, 50}, **PlotPoints** → 50, **PlotRange** → **All**, **Mesh** → **None**, **AxesLabel** → {"N", **Subscript**["n", "th"], "R"}, **PlotStyle** → **Directive**[**Blue**, **Opacity**[0.5]]]

**In[111]=** **Show**[**Comp**]

